Aalborg Universitet

Fabricating B-cyclodextrin based pH-responsive nanotheranostics as a programmable polymeric nanocapsule for simultaneous diagnosis and therapy

Zarepour, Atefeh; Zarrabi, Ali; Larsen, Kim Lambertsen

[Link to publication from Aalborg University](#)

ORIGINAL RESEARCH

Fabricating β-cyclodextrin based pH-responsive nanotheranostics as a programmable polymeric nanocapsule for simultaneous diagnosis and therapy

Atefeh Zarepour[1]
Ali Zarrabi[1]
Kim Lambertsen Larsen[2]

[1]Department of Biotechnology, Faculty of Advanced Sciences and Technologies, University of Isfahan, Isfahan, Iran; [2]Department of Chemistry and Bioscience, Faculty of Chemistry, Aalborg University, Aalborg, Denmark

Background: Fabrication of a smart drug delivery system that could dramatically increase the efficiency of chemotherapeutic drugs and reduce the side effects is still a challenge for pharmaceutical researchers. By the emergence of nanotechnology, a huge window was opened towards this goal, and a wide type of nanocarriers were introduced for delivering the chemotherapeutic to the cancer cells, among them are cyclodextrins with the ability to host different types of hydrophobic bioactive molecules through inclusion complexation process.

Aim: The aim of this study is to design and fabricate a pH-responsive theranostic nanocapsule based on cyclodextrin supramolecular nano-structure.

Materials and methods: This nanostructure contains iron oxide nanoparticles in the core surrounded with three polymeric layers including polymeric β-cyclodextrin, polyacrylic acid conjugated to sulfadiazine, and polyethylenimine functionalized with β-cyclodextrin. Sulfadiazine is a pH-responsive hydrophobic component capable of making inclusion complex with β-cyclodextrin available in the first and third layers. Doxorubicin, as an anti-cancer drug model, was chosen and the drug loading and release pattern were determined at normal and acidic pH. Moreover, the biocompatibility of the nanocapsule (with/without drug component) was examined using different techniques such as MTT assay, complement activation, coagulation assay, and hemolysis.

Results: The results revealed the successful preparation of a spherical nanocapsule with mean size 43±1.5 nm and negatively charge of −43 mV that show 160% loading efficacy. Moreover, the nanocapsule has an on/off switching release pattern in response to pH that leads to drug released in low acidic pH. The results of the biocompatibility tests indicated that this nano drug delivery system had no effect on blood and immune components while it could affect cancer cells even at very low concentrations (0.3 μg mL^{-1}).

Conclusion: The obtained results suggest that this is a "switchable" theranostic nanocapsule with potential application as an ideal delivery system for simultaneous cancer diagnosis and therapy.

Keywords: nanocapsule, host-guest interaction, on/off switching, pH-responsive, smart nanocarrier

Correspondence: Ali Zarrabi
Department of Biotechnology, Faculty of Advanced Sciences and Technologies, University of Isfahan, Isfahan 81746-73441, Iran
Tel +98 313 793 4360
Fax +98 313 793 2342
Email a.zarrabi@ast.ui.ac.ir

Introduction

Finding an effective method for the treatment of cancer, as an incurable, progressive illness, has attracted lots of attention. Conventional chemotherapy, as one of the most frequently used methods for cancer treatment, is carried out based on non-targeted drug delivery to cancer cells that in turn, is associated with undesirable

side-effects on normal cells. In fact, the common anti-cancer drugs have several drawbacks, including poor water solubility, immune system activation, and fast elimination from the body, leading to insufficient delivery to the tumors and suboptimal therapeutic activity. Therefore, design and fabrication of a drug delivery system with prominent properties for cancer therapy is the aim of variety of researches.[1–5]

The emergence of nanoscience and nanotechnology created many hopes for the treatment of various diseases through the introduction of novel strategies. One of the most interesting fields of nanotechnology in medicine and pharmacology is the fabrication of nanocarriers for specific delivery of drugs to the target site. These nanocarriers are classified in certain categories and can act as a mask for the drugs leading to an increase in the bioavailability of the drugs by protecting them from blood clearance through immune system factors.[6–9]

Using stimuli triggers introduce a new class of carriers entitled smart nano-systems, which could release their cargo in response to a specific physiological feature, at the appropriate time, right site and suitable dose. These stimuli trigger are categorized into three main classes: chemical (pH, ionic strength), physical (light, magnetic, and temperature) and biological (enzymes, and receptor) stimulation. The unique property of smart delivery systems in releasing their drug cargo in the presence of a specific condition could increase the therapeutic efficiency along with decrease in the side effects of the drugs.[10–13]

Integrating therapeutic properties of these types of nano-systems with diagnosis features could lead to produce multifunctional nanocarriers recognized as smart nano-theranostics. Nano-theranostics are a class of nano-systems with the ability of simultaneous diagnosis and therapy, in which the diagnostic material emerges as the therapeutic agent itself or in combination with a therapeutic species. So far, several types of nanomaterials have been introduced with the ability to enhance the quality of imaging techniques like magnetic nanoparticles in magnetic resonance imaging (MRI), gold nanoparticles in computed tomography (CT), and graphene oxide nanosheets and quantum dots in fluorescence diagnosis.[14–17]

Among different types of nanocarriers, hollow nanocapsules are one of the most important classes, which consist of a hole surrounded by one or more polymeric shells in the size of nanometers (10–1000 nm), that have the ability of drug entrapment in their internal space. There are several methods for the preparation of nanocapsules including nano-precipitation, emulsion–diffusion, template-based method, double emulsification, emulsion-coacervation, polymer-coating, and layer-by-layer (LbL).[18–23] LbL, which was proposed by Sukhorukov and his co-worker in 1998, is known as one of the most promising techniques for nanocarrier formation. This method is based on assembling multilayers, usually with the opposite charges, on the surface of an organic or inorganic template which will be removed by the use of etching procedures to produce hollow capsules with multilayer shells.[24,25]

Recently, application of cyclodextrin (CD) and its derivatives for the preparation of different types of nanosystems has attracted lots of attention. β-cyclodextrins (βCDs) are cyclic oligosaccharides consisting of α-(1–4) inked- glucopyranose units that has a symmetrical form resembling a truncated cone. The specific structure of βCD with hydrophobic inner cavity and hydrophilic surface makes it a promising candidate for drug delivery systems. In fact, the inclusion complex formed between hydrophobic drugs as guests and the cavity of CD as the host is widely used for drug delivery purposes. This feature not only could be used for formulating hydrophobic drugs, but could also be applied for production of supramolecular structures like nanosponge and nanocapsules.[26–28]

Sulfadiazine (SDN) is a type of sulfonamide family, a group of anti-bacterial and anti-fungal drugs with the ability of infection treatment. SDN has a similar structure with para-aminobenzoic acid, which is necessary for bacterial folic acid synthesis pathway and thus could stop the synthesis procedure by inhibition of dihydropteroate activity. The low water solubility and chemical structure of this drug make it a good candidate for interaction with the hydrophobic cavity of βCDs. Moreover, due to its molecular features, it can show a pH-responsive behavior.[29–31]

Based on the data mentioned above, in this research, it is intended to fabricate a new pH-responsive polymeric nanocapsule through the LbL method. For this purpose, Fe_2O_3 nanoparticles were synthesized and covered with Au nano-shell through Lyon's method.[32] Then, this core-shell nanoparticle was used as a template for loading three polymeric layers on its surface, which was done through exploiting the inclusion complex formation between βCD available in the first and the third layers and partially hydrophobic SDN existed in the second layer. The first layer consisted of thiolated βCD attached on the surface of Au through self-assembly method. Polyacrylic acid (PAA) conjugated with the SDN, as a pH-responsive agent, was used as the second layer constituent forming inclusion

complexes with βCDs of the first layer. In the third layer, βCD functionalized polyethylenimine was used to make inclusion complex with remaining SDNs. The presence of polymeric structure in the second and the third layer is critical since they can maintain the structural sustainability of the nanocapsule. At the final step, of nanocapsule fabrication, the Au shell was removed to prepare the whole structure of the nanocapsule. Different types of characteristic analysis (FTIR, UV-Visible spectroscopy, FE-SEM, EDX, NMR, XRD, and Zeta potential) were conducted to evaluate the successful synthesis of the nanocapsule. Then, doxorubicin (DOX) as a hydrophilic, anti-cancer drug was loaded into the nanocapsule and the drug loading and release pattern of nanocapsule were assessed in response to pH (7.4 and 6.6). At the end, the biocompatibility of the nanocapsules (with and without drug) was evaluated by cytotoxicity and hemocompatibility (coagulation, complement activation, and hemolysis) tests.

Materials and methods
Materials

$FeCl_2.4H_2O$ and $FeCl_3.6H_2O$ were purchased from Merck, Germany. $HAuCl_4.3H_2O$, tetramethylammonium hydroxide (TMAOH), sulfadiazine, PAA (Mw=1800 g mol-1, R & D application), (1-Ethyl-3-(3-dimethylaminopropyl) carbodiimide hydrochloride (EDC), polyethylenimine (PEI), Iodine, and potassium iodide were received from Sigma, USA. 4-Dimethylaminopyridine (DMAP), sodium borohydride, epichlorohydrin, sodium citrate, cystamine dihydrochloride, hydroxylamine hydrochloride, dimethyl sulfoxide (DMSO) and dimethylformamide (DMF) were obtained from Merck, Germany. MCF-7 and L-929 cell lines were purchased from Pasteur Institute of Iran, Tehran, Iran.

Methods
Preparation of nanocapsule
Iron oxide synthesis

Fe_3O_4 nanoparticles were synthesized using the co-precipitation method.[33] Briefly, $FeCl_2.4H_2O$ and $FeCl_3.6H_2O$ were dissolved in degassed HCl (0.4 M) and were then rapidly added to 375 mL of ammonia solution (0.7 M). The reaction solution should be mechanically stirred under N_2 atmosphere for about 30 mins at 45 °C by adjusting the pH around 10. Then, the synthesized nanoparticles were collected using neodymium magnet, washed several times

with deionized water (DI-water) and ethanol and dried with freeze-dryer (VaCo5, Zirbus, Germany).

Maghemite nanoparticles were then synthesized by oxidation of Fe_3O_4 nanoparticles. For this purpose, Fe_3O_4 nanoparticles were sonicated in a solution of HNO_3 (0.4 M) for about 30 mins and then were refluxed in HNO_3 (0.04 M) at about 300 °C for 2 hrs. At the end, the reddish-brown nanoparticles were collected by the magnet, washed several times with DI-water and dried by using freeze-dryer.[32]

Fabrication of Fe_2O_3@Au core-shell nanoparticles

Fe_2O_3@Au nanoparticles were synthesized based on Lyon's iteration method with little modifications.[34] It should be noted that Au has very low tendency to attach to the surface of Fe; therefore iron oxide nanoparticles need a pre-treatment step to be prepared for coating with Au shell. For this, the nanoparticles were dissolved in a solution of TMAOH (0.1 M) for at least one night in a concentration of about 36 mM. Then, a diluted solution of nanoparticles (1.1 mM) was mixed with the same amount of sodium citrate (0.1 M) for about 20 mins. After that, this solution was diluted 20 fold with the addition of DI-water and TMAOH and then different amounts of $NH_2OH \cdot HCl$, 0.2 M (750, 250, 250, 250, 250 μl) and $HAuCl_4$, 1% (625, 500, 500, 500, 500 μl) were added to this solution during five consecutive iterations with 30 mins interval times.

Synthesis of the first polymeric layer (L1)

The first polymeric layer was consisted of a specific amount of thiolated-βCD (βCDSH) polymerized on the surface of Fe_2O_3@Au nanoparticles. The βCDSH was produced in a two-step mechanism; at first, βCDs were tosylated using para-toluenesulfonyl chloride to achieve mono-6-tosyl-β-cyclodextrin. In detail, 2 gr of βCDs were dispersed in 28 mL DI-water, then 6 mL of NaOH solution was added drop-wise to dissolve the βCD. The tosylation reaction was occurred during a 5 h interaction between the above solution and para-toluenesulfonyl chloride (500 mg). The final solution was filtered to remove non-reacted tosyl reagents, and tosylated-βCDs (Tos-βCDs) were separated by the addition of cationic resins in ice-bath.[35]

At the next step, Tos-βCDs were reacted with cystamine dihydrochloride in a mixed solution of water: DMSO (1:1), at 70 °C for 72 h. The results of this reaction were exposed to 1ml of sodium borohydride (2.6 mmol) that reduced the disulfide bond of the cystamine and produced βCDSH (Scheme 1).[36,37]
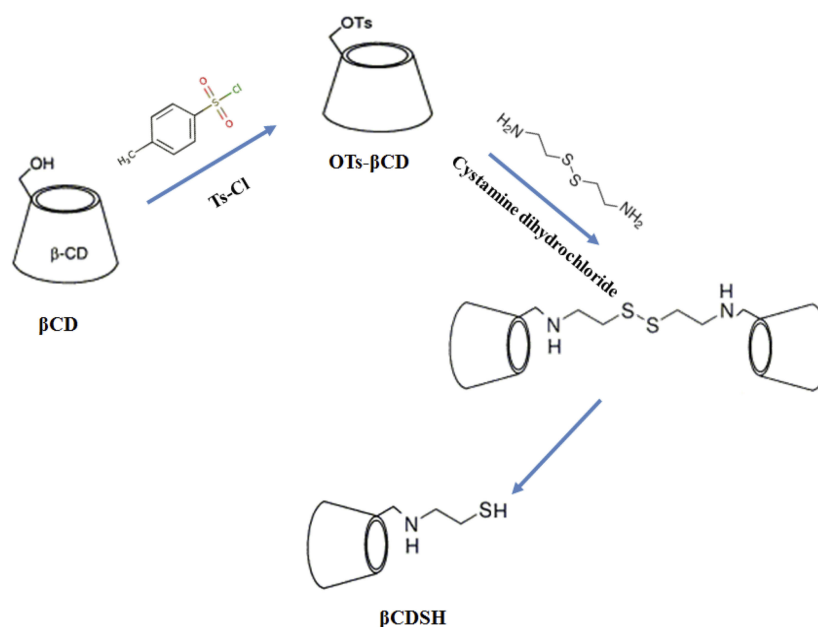
Scheme I Two step production of βCDSH.

The monomeric βCDSH species were then attached to Fe₂O₃@Au nanoparticles through a self-assembling reaction during 24 h at room temperature. Then, the polymerization reaction was conducted on the surface of nanoparticles using epichlorohydrin as the cross-linker. The final product was separated by the magnet, washed with DI-water and dried by freeze-dryer.

Synthesis of the second polymeric layer (L₂)

The second polymeric layer contained a pH-responsive reagent which could form host-guest interactions with βCD. It was prepared through a mediation reaction between SDN and PAA with the aim of EDC/DMAP as coupling agents. Briefly, 1 mmol of PAA was dissolved in 40 mL DMF. After 10 min, SDN (8 mmol) was added to the mentioned solution, DMAP (1.5 mmol) and EDC (3 mmol) were then added with about 15 mins interval time, respectively. The final solution was stirred for about 48 h at room temperature, precipitated in water and dried after washing several times with DI-water.

Synthesis of the third polymeric layer (L₃)

In the third layer, the linear form of polyethylenimine (L-PEI) was used as a backbone for the attachment of βCDs. For this, 4 gr of Tos-βCD was reacted with the amine groups of polymer L-PEI (500 mg) in 36 mL DMSO for seven days. The final product was precipitated in the presence of excess amounts of acetone and dialyzed against water for another seven days to remove non-reacted components.[37]

Fabrication of self-assemble nano-system

To prepare the nano-system, an aqueous solution of Fe₂O₃@Au/PβCD nanoparticles was added dropwise to the solution of L₂ in DMSO, and the final reaction mixture was magnetically stirred for 2 days. Then, the nanoparticles were collected by a magnet, washed with DI-water to remove unreacted materials, and after 2 h keeping in −20 °C, dried with freeze-drier to tight the reaction of βCDs and SDNs. In the next step, an aqueous solution of Fe₂O₃@Au/PβCD/PAA-SDN was added to the aqueous solution of PEI-βCD, dropwise, stirred for 48 h and dried the same as described for the previous step.[38]

Au layer removal

Finally, the nanocapsule was prepared through the Au layer removal using a solution of potassium iodide and extra amounts of iodine in water.[39] Using excess amounts of iodine prevented the decomposition of unstable gold iodide. The Au depleted nanocapsules were then separated by a magnet, washed several times with DI-water to remove excess iodine and dried with freeze-dryer.

Characterization

Different types of physicochemical analysis were used to characterize the nanocapsule in the different fabrication steps. FTIR spectroscopy (400–4000 cm⁻¹) was chosen to evaluate the surface characteristics of each layer and also inclusion complex formation (JASCO 6300 spectroscope,

Japan, transmission mode). The crystalline structure of nano-particles and host-guest interaction were evaluated by XRD (Bruker diffractometer with Cu Kα radiation, Germany). To assess the effect of each Au addition iterations on shell formation, UV-Visible spectroscopy (V670, Japan) was utilized. Size, morphology, and elemental composition of the nanocapsules were determined by FE-SEM/EDX (MIRA3 TESCAN, Czech Republic). In addition, H-NMR (Bruker Ultrasheet-400 MHz Spectrometer, Germany) was selected to confirm the production of polymeric layers. The charge of the nano-system after the addition of each layer was also assessed by Zeta potential (HORIBA, scientific SZ100, Japan).

Drug loading determination

DOX is a typical hydrophilic drug that is widely used for the treatment of various types of cancers. It can affect the cancer cells by intercalating the nucleus DNA through blocking gene replication and transcription. The rapid elimination of the drug from the body, as well as its nonreversible side effects, shed light on the importance of using nanocarrier for its delivering to the targeted site.[40,41]

DOX loading was done in three different mass ratios of drug (D): nanocapsule (N) (2:1, 1:1 and 1:2) in phosphate buffer saline (PBS) in two different pH (6.6 and 7.4). After 24 h of drug exposure with nanocarrier at room temperature, the loaded nanocarriers were collected with a magnet, washed with PBS to remove unloaded drugs and dried with freeze-dryer.

The amount of unloaded drug was determined by measuring the absorbance of the supernatant at 490 nm using UV-Visible spectrophotometer, then the percentage of loading and entrapment efficiency of the drug were calculated based on Equation (1) and (2), respectively:[42]

$$\% \, Loading \; Efficiency \; (LE) = \frac{Total \; DOX \; added \; (wt) - Unloaded \; DOX \; (wt)}{Total \; nanocarrier \; (wt)} \quad (1)$$

$$\% \, Entrapment \; Efficiency \; (EE) = \frac{Total \; DOX \; added \; (wt) - Unloaded \; DOX \; (wt)}{Total \; DOX \; added \; (wt)} \quad (2)$$

Ph-responsive drug release

The pH-responsive release profiles of selected drug-loaded nanocapsules were assessed at 37 °C during 14 days. For this purpose, specific amounts of drug-loaded nanocapsules were dispersed in 1.5 mL PBS with two different pH of 7.4 and 6.6, which were selected based on the normal pH of the body and pH of tumor tissues,

respectively.[43] After an appropriate time, nanocapsules were collected by a magnet, and the amounts of drug released were determined by comparing the absorbance of the supernatant with the standard curve.

Biocompatibility tests
MTT assay

The cytotoxicity of the nanocapsules (with/without drug molecules) was evaluated by MTT assay. For this purpose, MCF-7 and L929 cells were selected as cancerous and normal cell lines, respectively. Cells were cultured in Dulbecco's Modified Eagle Medium (DMEM) medium in 96 well plates with the concentration of 10,000 cells per well and incubated for 24 h in 4.5% CO_2 atmosphere at 37 °C. After that, different concentrations (0.1, 0.2, 0.3, 0.4 and 0.5 μg mL^{-1}) of drug-loaded nanocapsules in media were exposed to cells for 24 and 48 h. Moreover, specific amounts of free drugs (as positive control) and nanocapsule (without drug) were also subjected to the cells. After 24 and 48 h, the medium of each well was discarded, cells were washed with PBS and then 100 μl of fresh media with 10 μl MTT solution (5 mg mL^{-1} in PBS) was added to each well. After 4 h incubation at 37 °C, the supernatant of each well was replaced with 100 μl DMSO and cells were incubated for another 1 h. During this process, the MTT salt was converted to an insoluble component, formazan, via an enzymatic reaction done in the mitochondria of the living cells. The produced formazan was then solubilized by the addition of DMSO and the absorbance of each well was determined at 493 nm using ELISA reader (Bio-Rad, USA).

Hemolysis assay

To evaluate the hemolytic effect of nanocapsules (with/without drug) on the red blood cells (RBCs), 3 mL of the blood sample in EDTA-contained tube (from a volunteer with ethical permissions) was centrifuged for 5 mins at 1600 RPM to separate the RBCs from other parts of the blood. The precipitate RBCs of the blood sample were then washed three times with PBS and centrifuged to remove any hemolytic contaminant. Then, 200 μl of the sedimented RBC was dispersed in 3.8 mL of PBS. After that, 200 μl of this solution was added to 800 μl of nanocapsule solution (with different concentrations). DI-water and PBS were used as positive and negative controls, respectively. The samples were kept at room temperature for about 3 h and then were centrifuged at 1600 RPM for 5 mins. The absorbance of the supernatant was measured at 541 nm and the amount of hemolysis was calculated using Equation 3:[44]

$$\% \, of \, Hemolysis = $$
$$\frac{Absorbance \, of \, sample - Absorbance \, of \, negative \, control}{Absorbance \, of \, positive \, control - Absorbance \, of \, negative \, control}$$
(3)

Complement activation

The complement system is a part of the immune system contains at least 35 proteins that can be stimulated in response to any foreign material that enters the body and eliminates it through three main pathways: classical, alternative and lectin route. Stimulation of each of these systems can limit the foreign materials through the attachment of these proteins on the surface of the material or/and by activating the opsonins of the immune system.[45] Two main components of this system that are evaluated in blood tests are C_3 and C_4 proteins. Based on this, in this research, different concentrations of nanocapsules (with/without drug) were exposed to blood plasma and their effects on the activation of C_3 and C_4 proteins were evaluated by using a commercial single radial immunodiffusion (SRID) immunoassay kit.[46]

Coagulation assay

Coagulation is one of the other eliminating mechanisms of the immune system for the foreign materials in which the activation of a cascade of several factors through two main intrinsic and extrinsic pathways will lead to cross-linked fibrin clot formation. Based on this, here the effect of the nanocapsules on the intrinsic and extrinsic pathways of the coagulation system was evaluated by quantitative measurement of the change in the prothrombin time (PT) and activated partial thromboplastin time (APTT). To this end, specific amounts of platelet poor plasma were exposed to different concentrations of nanocapsules (with/without drug) and were incubated at 37 °C for about 30 mins. Then the activation time was measured after addition of Innovin (as the activator of extrinsic pathway), and actin and calcium chloride (the activators of intrinsic pathways).[47]

Statistical analysis

SPSS software (version 21, parametric analysis of variance [ANOVA (Tukey)]) was used for quantitative data analysis and results are reported as mean values ±standard deviation (SD) with significant value at $P \leq 0.05$.

Results

Fabrication of iron oxide nanoparticles

Monodispersed maghemite nanoparticles were synthesized by oxidation of Fe_3O_4 nanoparticles. For this purpose, the Fe_3O_4 nanoparticles were oxidized in the presence of diluted nitric acid that led to the preparation of reddish-brown nanoparticles from the primary black ones. The fabrication of magnetic nanoparticles was confirmed by using different analytical tests. The FE-SEM result of γ-Fe_2O_3 is shown in Figure 1. It is evident from the figure that the γ-Fe_2O_3 nanoparticles have monodispersed spherical shape with 19 ±2 nm size. Moreover, the formation of γ-Fe_2O_3 nanoparticles was also evaluated by using other techniques such as FTIR and XRD, the result of which are reported in the supporting information as Figures S2 and S3.

Synthesis of fe₂o₃@au core-shell nanoparticles

For preparation of Au coated Fe_2O_3 nanoparticles, a solution of 1.1 mM γ-Fe_2O_3 was mixed with sodium citrate for at least 20 mins. During this process, the activated surface of the iron oxide nanoparticles was modified with citrate groups that act as a thin layer coating on the surface of magnetic nanoparticles to prepare them for Au reception, as well as, being a critical reagent for the Au shell reduction process. After dilution of the above solution, $HAuCl_4 \cdot 3H_2O$ in combination with the reducing agent ($NH_2OH \cdot HCl$) was added in five iterations resulting in the fabrication of a thick shell on the surface of nanoparticles. By addition of the first iteration, the color of the solution changed from light brown to dark purple (Figure 2A) confirming the production of Au nanoparticles. In the first iteration, the prepared Au nanoparticles were most likely deposited on the surface of the nanoparticles in an
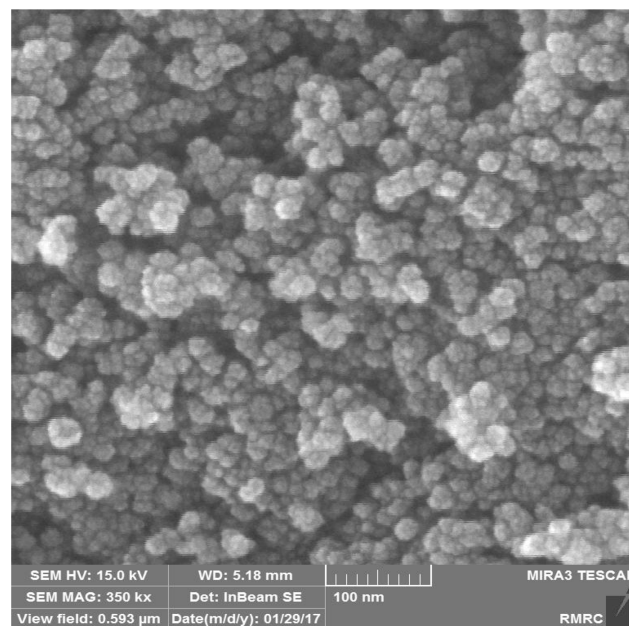

Figure 1 FE-SEM analysis of γ-Fe_2O_3.
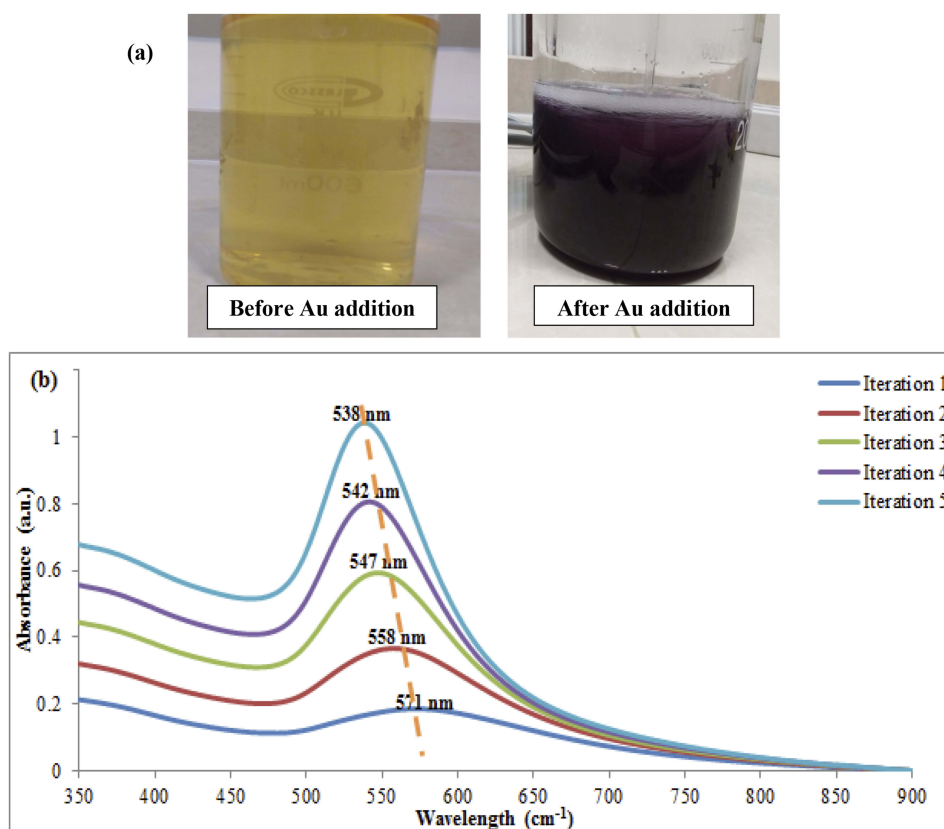
Figure 2 (**A**) Changing the solution color before and after of Au addition, (**B**) UV-Visible spectroscopy of five Au iterations.

island pattern which was then converted to a complete shell by proceeding of the next iterations. This feature was confirmed by the results of UV-Visible spectroscopy in which a blue shift was observed after the addition of each iteration (Figure 2B). In other words, the blue shift of the UV-Visible spectrum revealed that the morphology of the coated nanoparticles was gradually changed to a uniform spherical shape during each addition, a phenomenon that also could be approved by a significant decrease in the broadening of the peaks.[48]

The spherical shape of the core-shell nanoparticles was also confirmed through the result of FE-SEM imaging. As it is shown in Figure 3A, coating Au on the surface of nanoparticles turned to decrease the aggregation of the nanoparticles and resulted in nanoparticles with mean size of 36 ±4 nm. Moreover, the chemical composition of the template was assessed by Energy Dispersive X-ray (EDX) spectroscopy. The presence of Au and Carbon atoms confirmed the gold coating on the surface of iron oxide nanoparticles (Figure 3B). The successful coating of magnetic nanoparticles with Au shell was also revealed by the crystal structure of the nanoparticles (XRD) (Figure 3C), in which peaks at

around 45°, 52°, 77° and 93.5° could be indexed to (111), (200), (220) and (311) planes of gold cubic and weak peaks at 36°, 42°, 51° and 75° could be indexed to (200), (311), (002) and (102) planes of γ-Fe_2O_3 (based on Joint Committee on Powder Diffraction Standards, JCPDS 04–0784 and JCPDS 39–1346, respectively).[49]

Preparation of nanocapsule

As mentioned previously, the nanocapsules were consisted of a template with three polymeric layers. In the first layer, βCDSH components were attached on the surface of the Au shell through self-assembly driving force and then, they were polymerized using epichlorohydrin. During the polymerization reaction, the chlorine atom of the epichlorohydrin acts as a leaving group and by the interaction with the activated hydroxyl group of βCD, leads to the formation of a connection between βCD and epichlorohydrin through the ether bond. In the second step of this reaction, a ring-opening polymerization reaction occurred between the other side of epichlorohydrin and one another βCD component. The cascade reaction happened between the available
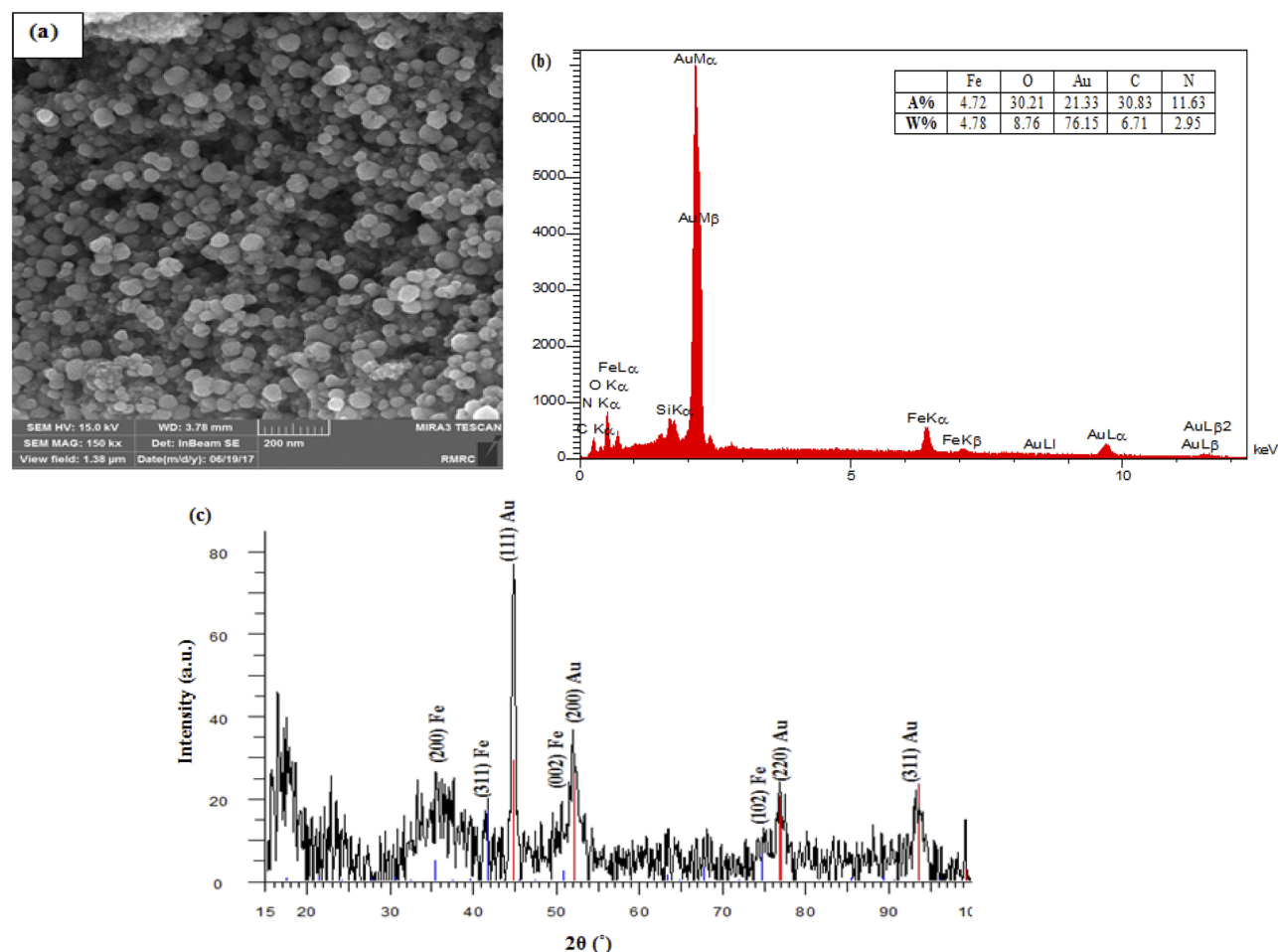
Figure 3 (**A**) FE-SEM, (**B**) EDX and (**C**) XRD of γ-Fe₂O₃@Au core-shell nanoparticles.

βCD components and epichlorohydrin, leads to the production of a polymeric chain around the γ-Fe₂O₃@Au nanoparticles.[50]

The SDN functionalized PAA was selected as the second layer that was prepared through an amidation reaction. For this purpose, excess amounts of SDNs were exposed to the carboxyl groups of PAA in the presence of EDC and DMAP. Then, the inclusion complex between PAA-SDN and βCDs of the Fe₂O₃@Au/PβCD was formed within 72 h using the freeze-drying method.[51] In this process, the amino-hexagonal ring and the NH group of the SDN interact with the hydrophobic cavity of βCD (Scheme 2). Changing the pH of the surrounded environment induced a positive charge in this NH group leading to a partial exclusion of SDN from the cavity.

For the third layer, L-PEI polymer functionalized with βCDs was chosen. The attachment of PEI to Tos-βCDs was performed with the aim of EDC and DMAP. The as-prepared L₃ layer was loaded on the γ-Fe₂O₃@Au/PβCD/

PAA-SDN by using the freeze-drying method. Finally, the hollow nanocapsule was prepared by removing the Au core of the nano-system in the presence of a solution of KI and I₂. The first significant change that revealed the Au deletion was the color change of the samples from dark purple to light brown (Figure 4).

Characterization

Several types of physicochemical analysis were used to assess the fabrication of the nanocapsule and its components. The results of characterization tests of the polymeric layers can be found in supporting information (Figures S1-S6).

FTIR

Figure 5A shows the FTIR result of βCD polymerized on the surface of the γ-Fe₂O₃@Au template. The main difference between polymerized βCD and βCD alone is the presence of two peaks in the range of 2800–2900 cm^{-1}
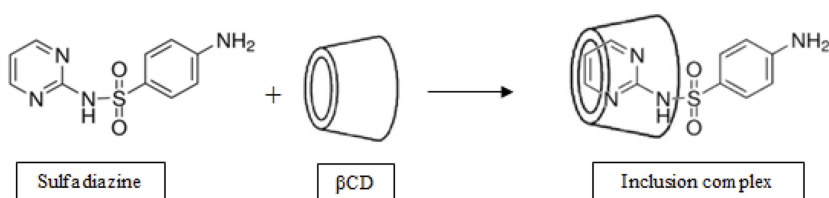
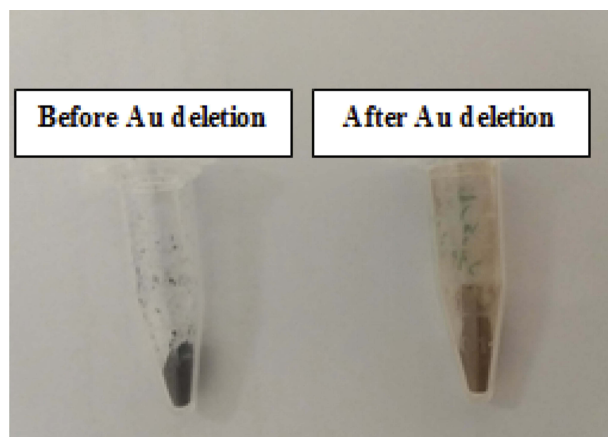**Scheme 2** The formation of an inclusion complex between βCD and SDN.

Figure 4 Change in the color of nano-system before and after removing the Au.

in the spectrum of polymerized βCD compared with one peak in the spectrum of βCD alone. Moreover, distinctive changes have occurred in the peaks mode of polymerized βCD in the range of 1200–1300 cm,$^{-1}$ which are associated to the CH stretching and bending vibrations. The other characteristic peaks in this curve are peaks at around 3400, 1040 and 580 cm^{-1} that are attributed to the OH and C-O-C stretching vibrations of polymerized nanoparticles, and Fe-O bond of γ-Fe$_2$O$_3$, respectively.[52] Moreover, the characteristic peak of thiol group at around 2550 cm^{-1} is also removed, which could confirm the successful attachment of βCDs on the surface of Au through a self-assembled monolayer bond.

By the addition of the second layer, the inclusion complexes between βCDs of the first layer and SDNs of L$_2$ were formed that was confirmed by the results of FTIR. For this, a comparison study was done between the curves of γ-Fe$_2$O$_3$@Au/PβCD, γ-Fe$_2$O$_3$@Au/PβCD/PAA-SDN, L$_2$ and physical mixture of the L$_2$, and γ-Fe$_2$O$_3$@Au/PβCD (Figure 5B). The FTIR spectrum of γ-Fe$_2$O$_3$@Au/PβCD/PAA-SDN has significant differences to that of γ-Fe$_2$O$_3$@Au/PβCD. In other words, the peaks at around 1690, 1640, 1450, 1370 and 1240 cm^{-1} which emerged in the spectrum of γ-Fe$_2$O$_3$@Au/PβCD/PAA-SDN, can be attributed to the amide bond, benzene ring, methyl groups and S=O groups of the L$_2$ layer, respectively. The appearance of Fe-O peak and also the redshift in the spectrum of γ-Fe$_2$O$_3$@Au/PβCD/PAA-SDN are the differences of this component with L$_2$. Finally, in comparison to the physical mixture, the intensity of the whole peaks of the γ-Fe$_2$O$_3$@Au/PβCD/PAA-SDN is dramatically decreased. Moreover, there are some peaks in the spectrum of the physical mixture, which are attributed to the βCD of the first layer and are disappeared in the γ-Fe$_2$O$_3$@Au/PβCD/PAA-SDN spectrum. Another critical point in the spectrum of γ-Fe$_2$O$_3$@Au/PβCD/PAA-SDN is the reduction of CN, aromatic amine and S=O peaks of SDN in comparison to the L$_2$ and physical mixture that can be attributed to the formation of inclusion complex.

As it was described previously, the interaction of the third layer with γ-Fe$_2$O$_3$@Au/PβCD/PAA-SDN occurred through inclusion complexation between βCDs of the third layer and the remaining SDN. The FTIR results of γ-Fe$_2$O$_3$@Au/PβCD/PAA-SDN/PEI-βCD, γ-Fe$_2$O$_3$@Au/PβCD/PAA-SDN, L$_3$, and physical mixture of γ-Fe$_2$O$_3$@Au/PβCD/PAA-SDN and L$_3$ are shown in Figure 5C. As can be seen in this figure, the spectrum of γ-Fe$_2$O$_3$@Au/PβCD/PAA-SDN/PEI-βCD follows the pattern of PEI-βCD with some slight differences that distinguish it from the spectrum of the L$_3$ and physical mixture. These differences include the presence of a Fe-O peak at around 580 cm^{-1} in the γ-Fe$_2$O$_3$@Au/PβCD/PAA-SDN/PEI-βCD curve and also a significant decrease in the intensity of the peaks. Moreover, the existence of βCD peaks at around 1250–1000 and 1650 cm^{-1} in the γ-Fe$_2$O$_3$@Au/PβCD/PAA-SDN/PEI-βCD spectrum, differentiate it from γ-Fe$_2$O$_3$@Au/PβCD/PAA-SDN spectrum. All these findings confirmed the fabrication of γ-Fe$_2$O$_3$@Au/PβCD/PAA-SDN/PEI-βCD from the interaction between L$_3$ and γ-Fe$_2$O$_3$@Au/PβCD/PAA-SDN.

Finally, by removing the Au core, a significant increase occurs in the intensity of the whole curve. Moreover, by the elimination of Au from the core of the nano-system, the characteristic peaks of L$_2$ and L$_3$ layers and also Fe-O
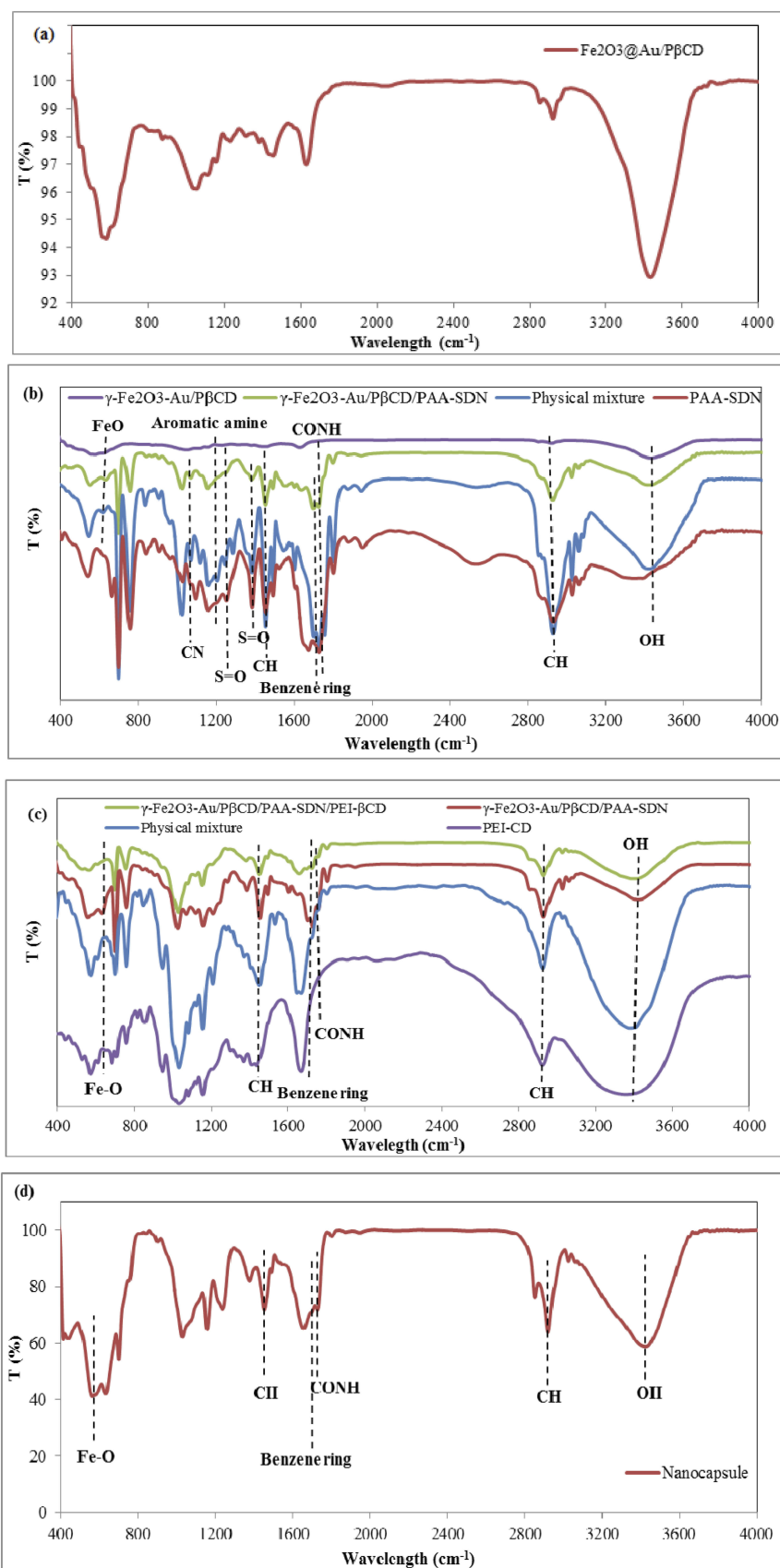
Figure 5 FTIR results of (**A**) γ-Fe$_2$O$_3$@Au/PβCD (**B**) γ-Fe$_2$O$_3$@Au/PβCD, γ-Fe$_2$O$_3$@Au/PβCD/PAA-SDN, physical mixture, PAA-SDN, (**C**) γ-Fe$_2$O$_3$@Au/PβCD/PAA-SDN, γ-Fe$_2$O$_3$@Au/PβCD/PAA-SDN/PEI-βCD, physical mixture, PEI-βCD, and (**D**) nanocapsule.

peaks of γ-Fe$_2$O$_3$ available in the core of nanocapsule are prominently increased (Figure 5D).

XRD

The probable differences in the crystallographic structure of nano-systems after the addition of each layer were investigated using XRD. By comparing the XRD result of γ-Fe$_2$O$_3$@Au/PβCD with that of γ-Fe$_2$O$_3$@Au, the polymerization of CD on the surface of nanoparticles was confirmed. In fact, a significant shift in the peaks of Au and Fe to the lower angles occurred in the spectrum of the γ-Fe$_2$O$_3$@Au/PβCD, so that the peaks which were attributed to the index planes of (111), (200), (220), and (311) of Au and (200), (311), and (102) of Fe showed a shift of about 7° to the lower degree. Moreover, an apparent reduction in the intensity of Fe and Au peaks, deletion of some Fe peaks and also the appearance of a broad peak in the range of 2θ=10–20°, which is appeared due to the amorphous structure of polymeric layer, could confirm the polymerization of βCD on the surface of nanoparticles (Figure 6A).

The preparation of inclusion complex was evaluated by comparing the XRD patterns of the γ-Fe$_2$O$_3$@Au/PβCD/PAA-SDN with PAA-SDN, γ-Fe$_2$O$_3$@Au/PβCD, and their physical mixture. The XRD pattern of PAA-SDN shows amorphous peaks at around 2θ=10–20° and 2θ=25–35°.[53] γ-Fe$_2$O$_3$@Au/PβCD/PAA-SDN has similar XRD pattern with the pattern of γ-Fe2O3@Au/PβCD except that in the spectrum of γ-Fe$_2$O$_3$@Au/PβCD/PAA-SDN the Fe index in 2θ=32° (200) is disappeared. This is an indicating difference between this sample and γ-Fe$_2$O$_3$@Au/PβCD and physical mixture, which suggests that this is due to the presence of PAA-SDN peak in this reign. Moreover, the presence of Au peaks in this spectrum in comparison to the PAA-SDN, confirmed the correct reaction between γ-Fe$_2$O$_3$@Au/PβCD and L$_2$ layers (Figure 6B).

In Figure 6C, the XRD pattern of the nano-system after the addition of the third layer is compared with γ-Fe$_2$O$_3$@Au/PβCD/PAA-SDN, L$_3$, and their physical mixture. By the addition of the third layer to the nano-system, the PAA polymeric peak at around 2θ=10–20° disappeared. Moreover, it could be seen that there are differences between the diffractograms of γ-Fe$_2$O$_3$@Au/PβCD/PAA-SDN/PEI-βCD, L$_3$ and γ-Fe$_2$O$_3$@Au/PβCD/PAA-SDN, suggesting the attachment of L$_3$ on γ-Fe$_2$O$_3$@Au/PβCD/PAA-SDN. Existence of difference between the curve of physical mixture and the third layer technically could reveal the inclusion complex formation. It is

necessary to mention that the several peaks exist in the spectrum of L$_3$ and physical mixture is attributed to the NaCl that was used in the purification step of the L$_3$ layer. However, these peaks disappeared in the spectrum of γ-Fe$_2$O$_3$@Au/PβCD/PAA-SDN/PEI-βCD due to the multiple washing steps before freeze-drying the sample.

Zeta potential analysis

The effect of each layer on the charge of the nano-system was evaluated by Zeta potential measurements (Table 1). The results revealed a positive charge for γ-Fe$_2$O$_3$ nanoparticles, which is due to the presence of HNO groups that were used for converting Fe$_3$O$_4$ to Fe$_2$O$_3$. Addition of Au shell changes the positive charge of the nano-system to negative because of the attendance of carboxylic acid groups of citrate. After addition of the first layer, the charge is dramatically decreased and reaches to about −39 mV, which could be attributed to the several hydroxyl groups of βCD moieties. By the addition of the second layer to the nano-system, the charge of the samples gets more negative value. The inclusion complex between βCD and SDN masks the nitrogen groups of SDN, which in turn could show positive charge before this complex; thus, the negative charges of the SO groups of SDN lead to the nano-system charge change to more negative charges. Finally, by addition of the third layer, which has several βCD components with large amounts of hydroxyl groups, the charge of nano-system gets more negative. These changes in charge of the nano-system after addition of different layers could be considered as evidence that confirmed the successful preparation of nanocapsule.

FE-SEM analysis

Changes in the size and morphology of the nano-system during the synthesis process were assessed using FE-SEM. Based on the results of Figure 7, nanoparticles have a spherical shape with the mean size 35.5±0.2, 40±2, 44±1.5 and 43 ±1.5 nm for γ-Fe$_2$O$_3$@Au/PβCD (Figure 7A), γ-Fe$_2$O$_3$@Au/PβCD/PAA-SDN (Figure 7B), γ-Fe$_2$O$_3$@Au/PβCD/PAA-SDN/PEI-βCD (Figure 7C), and hollow nanocapsules (Figure 7D), respectively.

EDX

Changes in the chemical composition of nanocapsule during the synthesis process were investigated by using EDX spectroscopy. The advent of sulfur and nitrogen peaks in the EDX diagram along with an increasing amount of carbon and oxygen atoms confirms the attachment of βCDSH on the surface of nanoparticles (Figure 8A). By the addition of the second and third layers, the amount of
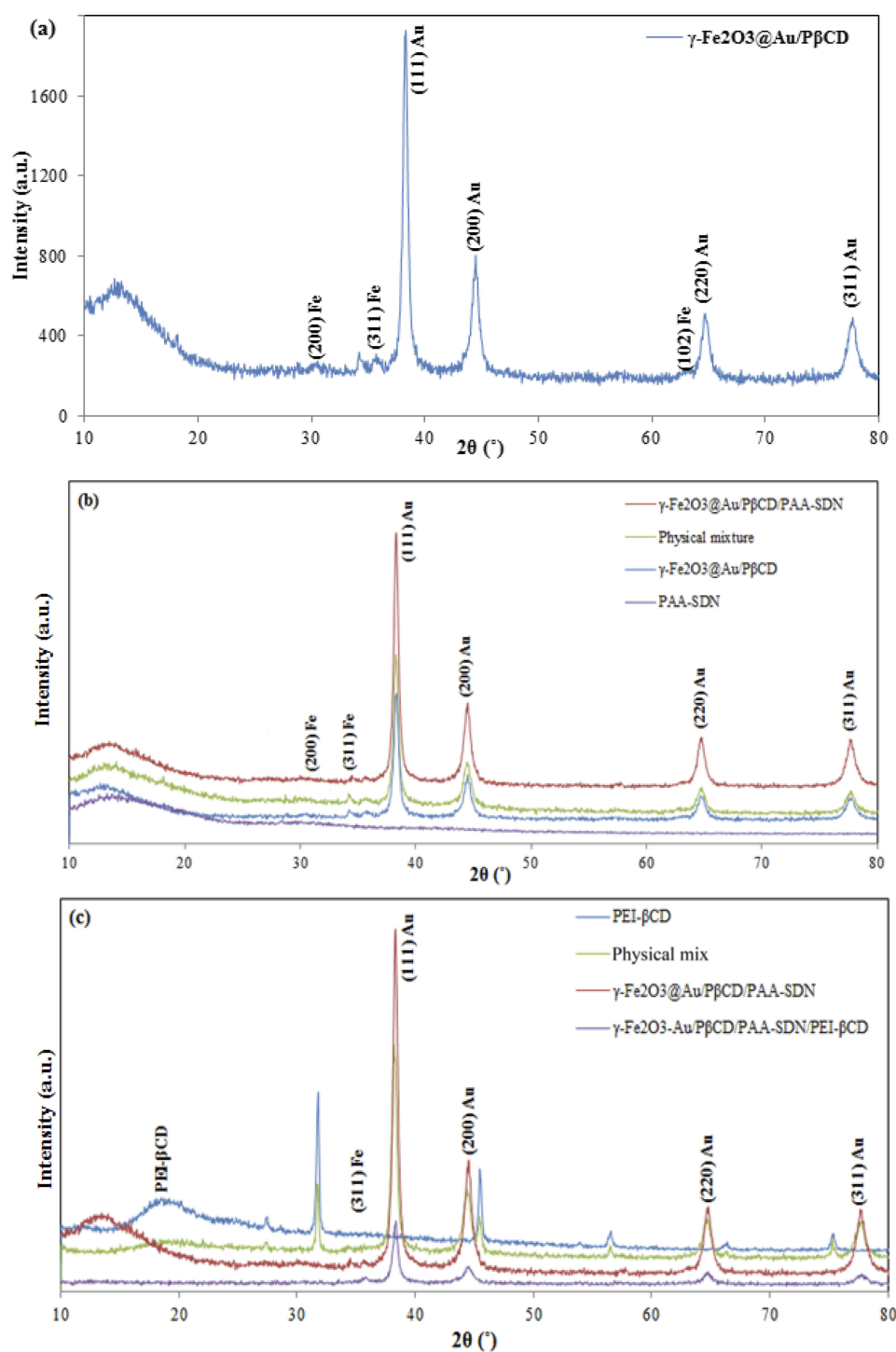
Figure 6 The XRD results of (**A**) γ-Fe$_2$O$_3$@Au/PβCD, (**B**) γ-Fe$_2$O$_3$@Au/PβCD, PAA-SDN, γ-Fe$_2$O$_3$@Au/PβCD/PAA-SDN, physical mixture of γ-Fe$_2$O$_3$@Au/PβCD and PAA-SDN and (**C**) γ-Fe$_2$O$_3$@Au/PβCD/PAA-SDN/PEI-βCD, γ-Fe$_2$O$_3$@Au/PβCD/PAA-SDN, PEI-βCD and physical mixture.

sulfur and nitrogen are also increased, confirming the presence of these layers in the sample (Figure 8B, C). Preparation of the hollow nanocapsule is accompanied by a significant reduction in the peaks of Au and also a dramatic increase in the peaks of Fe (Figure 8D).

Determination of loading and entrapment efficiency

Doxorubicin, as a widely used anti-cancer drug, was chosen and the loading behavior of the nanocapsule in response to changes to the pH of the surrounding

Table 1 Charge variation of the nano-system by addition of different layers

| Nanomaterial	Charge (mV)
Fe_2O_3	34.5
Fe_2O_3@Au	−11.6
Fe_2O_3@Au/PβCD	−38.9
Fe_2O_3@Au/PβCD/PAA-SDN	−40.3
Fe_2O_3@Au/PβCD/PAA-SDN/PEI-βCD	−42.3

environment was assessed. For this purpose, three different mass ratios of the drug to nanocapsule were dispersed in PBS in two different pH (6.6 and 7.4). The results of drug loading after 24 h are described in Table 2 confirming the effect of pH on drug loading efficiency of the nanocapsule. Based on the results, the amounts of drugs loaded at normal pH are more than the acidic one. Moreover, by increasing the mass ratio of drug to nanocapsule, the

loading efficiency is increased significantly so that in sample 3 and normal pH, it reaches to about 160% revealing an extraordinary capacity of this nanocapsule for drug loading of DOX.

The addition of drug molecules to the nanocapsule also leads to a dramatic increase in charge of nanocapsule from −42.8 to −28.9 (Figure 9) which is due to the positive charge of the drugs.

pH-responsive drug release

The pH-responsive drug release behavior of the nanocapsule was investigated in PBS with two different pH (7.4 and 6.6) at 37°C in three different mass ratios. After specific time intervals, the solution of each sample was replaced with a fresh solution, and the absorbance of each solution was read at 490 nm to determine the amount of released drug. The results of drug release are shown in
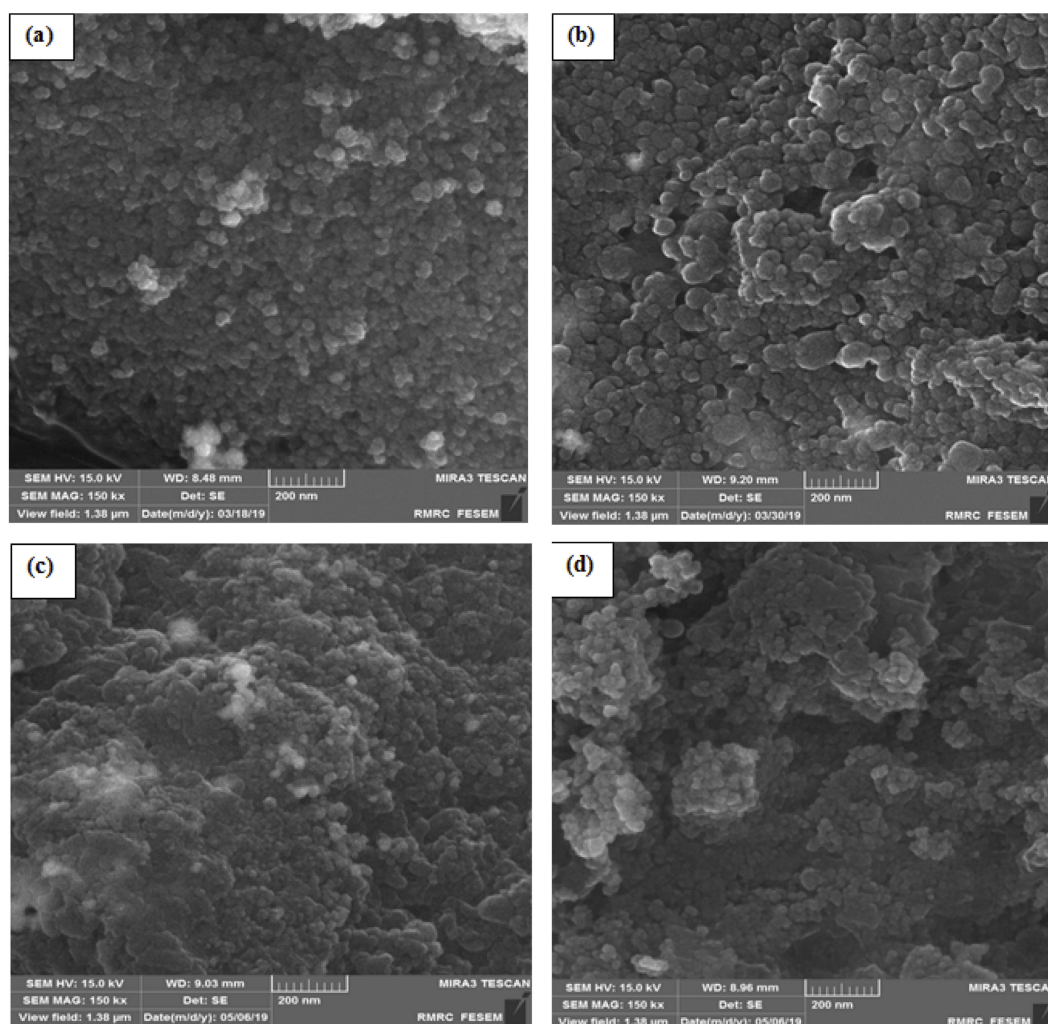
Figure 7 FE-SEM result of (**A**) γ-Fe_2O_3@Au/PβCD, (**B**) γ-Fe_2O_3@Au/PβCD/PAA-SDN, (**C**) γ-Fe_2O_3@Au/PβCD/PAA-SDN/PEI-βCD and (**D**) nanocapsule.
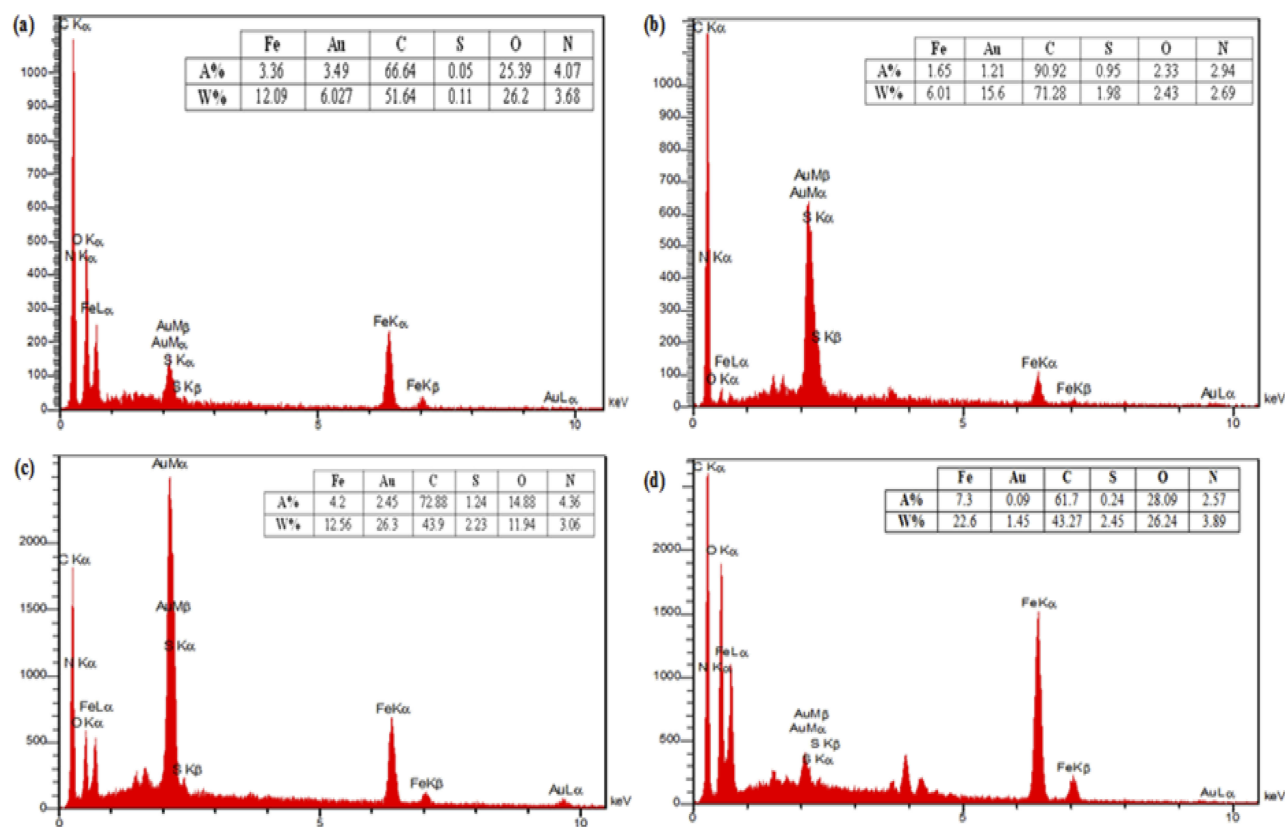
Figure 8 EDX analysis of (**A**) γ-Fe$_2$O$_3$@Au/PβCD, (**B**) γ-Fe$_2$O$_3$@Au/PβCD/PAA-SDN, (**C**) γ-Fe$_2$O$_3$@Au/PβCD/PAA-SDN/PEI-βCD and (**D**) Nanocapsule.

Table 2 Entrapment efficiency (EE) and the loading efficiency (LE) percentage of drug in nanocapsule at two pH with different mass ratios

Nanocapsule to Drug (N:D)			Sample 1 (N2:D1)	Sample 2 (N1:D1)	Sample 3 (N1:D2)
pH	**6.6**	%EE	74.31	85.55	76.67
		%LE	37.48	85.55	153.33
	7.4	%EE	85.50	90.91	79.40
		%LE	42.75	90.91	158.80

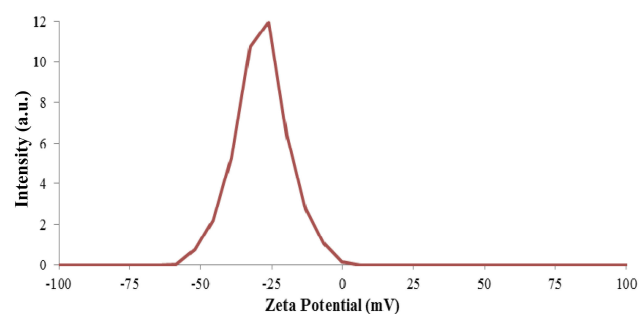**Abbreviations:** N, nanocapsule; D, drug.

Figure 9 Zeta potential curve of nanocapsule with drug.

Figure 10 (A–C). It can be recognized that all three samples show a pH-responsive behavior in their releasing pattern. Moreover, the release process follows a sustained release pattern so that drug release could be accomplished even after 14 days.

Based on the results, the most significant difference pH-responsive behavior is attributed to the sample 1 (Figure 10A) with about 74% drug released in acidic pH and about 33% in the normal condition during 14 days, which can be due to the presence of the low amount of drug molecules in this sample. In other words, the smaller amount of drug molecules in this case, not only turns to reduce the competition between the drug molecules, but also they are distributed in a larger volume of nanocapsule, and thus could be released in a more controllable state.

By increasing the amounts of entrapped drugs, the competition between drug molecules is increased;
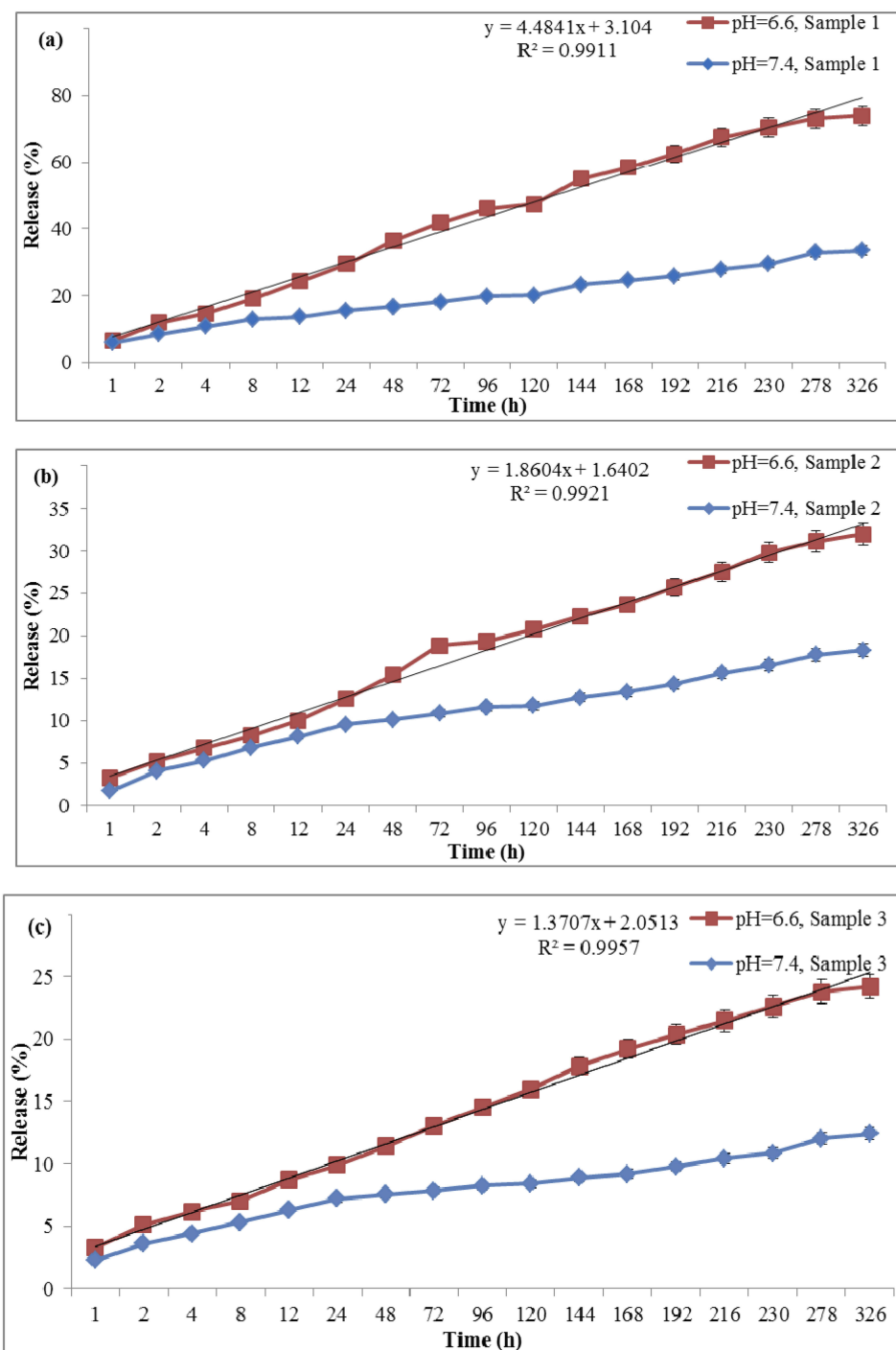
Figure 10 In vitro release profile of doxorubicin from (**A**) Sample, 1, (**B**) Sample 2 and (**C**) Sample 3, in PBS in two different pH 7.4 and 6.6.

preventing the burst release of drugs, as well as increasing the time of drug released (sample 2 (Figure 10B), and sample 3(Figure 10C)). Although these two samples have longer release time, the amounts of the released drug during 14 days, are the same or even higher than that of sample 1, which implies that they could show their toxicity effect during a more extended period of the time.

The other important point about this nanocapsule is that it shows an on/off switching behavior during the pH-responsive drug release. In other words, by changing the pH of the surrounding environment from normal to acidic, the SDNs located inside the cavity of cyclodextrin components partially exit, so the distance between three layers are increased, leading to an increase in the released drug in this acidic pH.

Biocompatibility tests

Based on the results of drug release, sample 1 and sample 3 were selected to evaluate the biocompatibility of the nano-system using different types of tests including MTT assay as cell viability assessment and hemolysis, coagulation and complement activation tests as hemocompatibility discernment.

MTT assay

One of the most critical tests that should be done before an in vivo application of a nano-system is the cell viability test to determine the cytotoxicity effect of the system. MTT assay, as one of the most common methods that is used for this purpose, is based on converting the MTT salt to an insoluble component, formazan, through a mitochondrial enzymatic reaction which is only carried out by living cells.[54]

The results of MTT assay of different nanocapsule concentrations (with/without drug) on MCF7 and L929 cell lines after 24 and 48 h are shown in Figure 11(A, B).

These results show that the drug-loaded nanocapsules have no significant effect on normal cells, even after 48 h (Figure 11A), while they show cytotoxicity against cancer cells after 48 h at concentrations of 0.4 and 0.5 μg mL^{-1} of sample 1 and concentrations above 0.2 μg mL^{-1} of sample 3 (Figure 11B). This is due to the changes that occurred in the pH of the cancer cell media, which is originated from their intrinsic property. In fact, cancer cells use the lactic acid pathway for creating ATP molecules that lead to change in the intracellular pH from normal to acidic form. These cells preserve their normal pH by excluding H$^+$ ions to the extracellular environment through specific ion-exchange channels that turn to the preparation of a low acidic microenvironment around the cells which can provide the best condition for the drug release from nanocapsule. It is necessary to mention that the higher amounts of drug released from sample 3 is the reason for the difference between the effective concentration of this sample and sample 1.

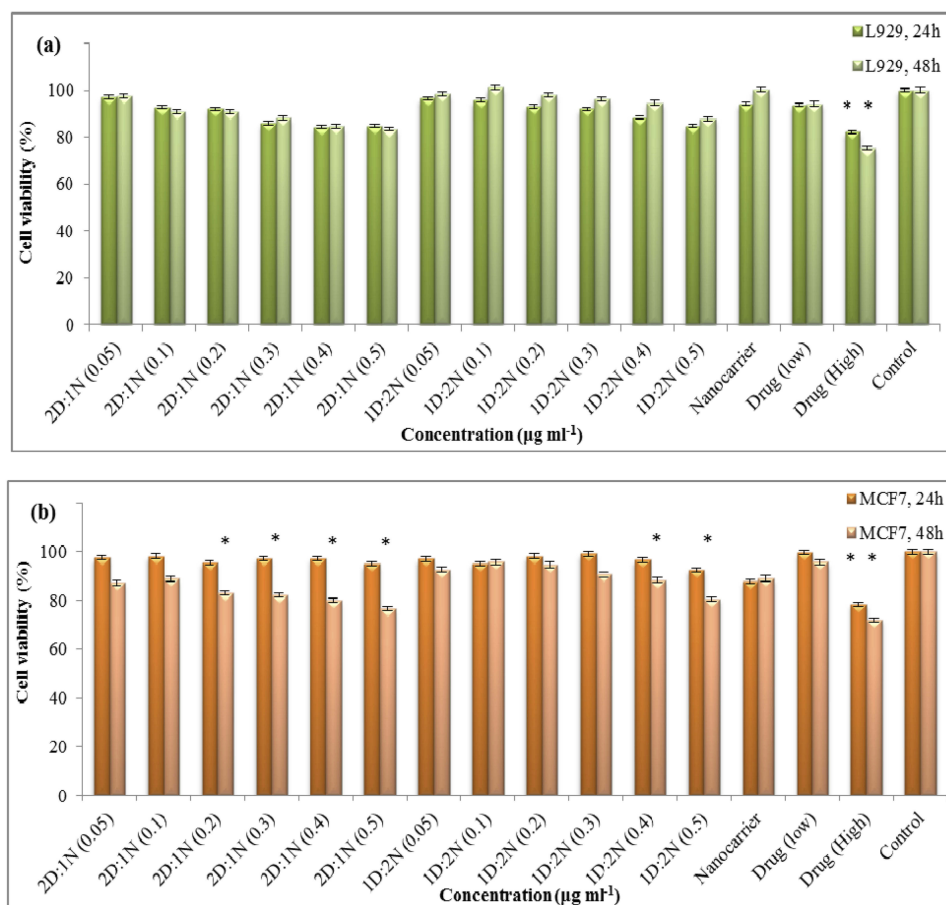The cytotoxicity of nanocapsule without the drug (in the concentration of about 0.5 μg mL^{-1}) was also tested and

Figure 11 Results of MTT assay on (**A**) L929 and (**B**) MCF-7 cell lines (*P≤0.05).

showed no cytotoxicity effect on the cells, revealing the cytocompatibility of the nanocapsule alone. Furthermore, the cytotoxicity of drug-loaded nanocapsule was compared with the free drug (with the same concentrations as the lowest and the highest amount of drug-loaded in the nanocapsule), and the results show the same cytotoxicity property as the loaded one. The results of this test were evaluated by statistical analysis (SPSS), and the significant samples are determined by "*" in the figures.

Based on the results of this test, the pH-responsivity of the nanocapsule could be confirmed by the appearance of cytotoxicity in cancer cells. Moreover, a brief comparison between the IC50 values of sample 1 and sample 3 (2 μM and 3μM, respectively) with that of free drug (9.8 μM), revealed that this nano-system shows an improvement in the therapeutic drug efficacy of doxorubicin.[55]

Hemolysis assay

The hemolytic behavior of the nanocapsule was evaluated by using hemolysis assay. For this purpose, different concentrations of sample 1 and 3 (0.1, 0.2, 0.3, 0.4 and 0.5) were exposed to RBC for a specific time, and then the percentage of hemolysis of each sample was determined by UV-Vis spectrophotometer. Both of the samples show the hemolytic activity of less than 1 percent (Figure 12), revealing that they have no hemolytic effect on RBC and thus it could be considered that they are hemocompatible (according to the American Society for Testing and Materials (ASTM F 756–00, 2000)).[56,57]

Complement activation

Evaluation of the complement activation, as part of the immune system, is one of the most important analysis for biomedical use of nano-systems. C_3, C_4, and C_5 are the most common components of this system that are usually assessed for determining the effect of foreign materials on complement activation. Herein, the drug-loaded/non-loaded nanocapsules were exposed with blood plasma and their effect on the activation of C_3 and C_4 were assessed by using specific kits. Results demonstrated that neither the drug-loaded nanocapsules nor the nanocapsules alone show no significant effect on the activation of complement components, which could confirm their hemocompatibility (Figure 13(A, B)). Statistical analysis also showed no significant differences between these samples compared to the control ($p \leq 0.05$).

Coagulation assay

The body uses several approaches for limiting foreign materials and removing them from the circulation system, one of which is clot formation that could be stimulated by activation of two main pathways; extrinsic and intrinsic. The effect of nanocapsules on these pathways was determined by calculating the prothrombin and thromboplastin activation time (PT and APTT) of platelet poor plasma. Results of coagulation assay (Figure 14(A, B)) confirmed that nanocapsules (with/without drug components) have no effect on the activation time of coagulation pathways and thus could be considered hemocompatible. The results of statistical analysis show no significant differences between the samples and the control ($p \leq 0.05$).

Discussion

Utilizing biological stimuli responsive manners have become one of the most important approaches for fabrication of therapeutic nano-systems, in particular nanocarriers for cancer drugs. These nanocarriers could deliver and release drug molecules just in the tumor tissue using an on/off switchable method. This means that they can selectively "switch on" in targeted cells and "switch off" in
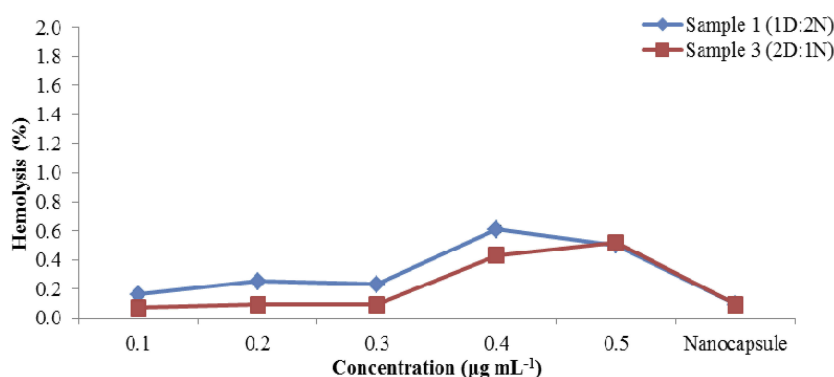

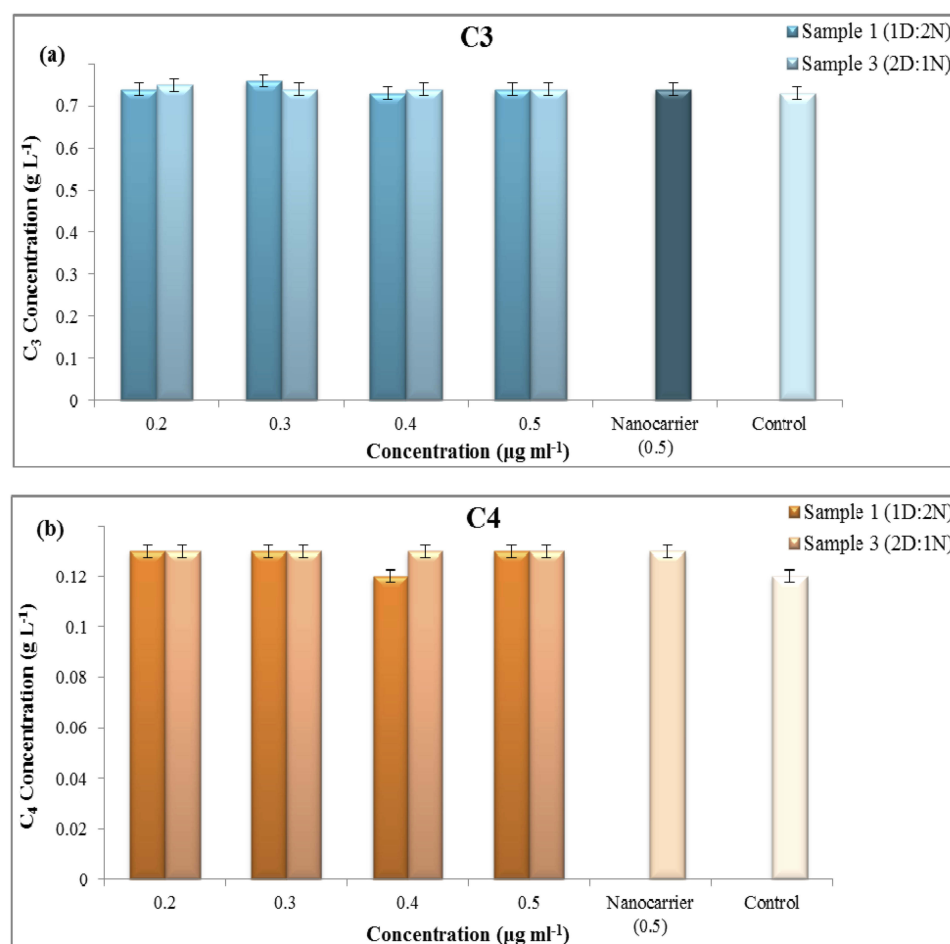**Figure 12** Hemolysis results of sample 1 and sample 3.

Figure 13 Effect of different concentrations of nanocapsule on (**A**) C_3, (**B**) C_4.

other tissues, and thus eliminating the toxic effects of drugs on healthy cells.[58]

Among different types of biological stimuli approach, pH-responsiveness is one of the most commonly studied functionalities for cancer therapy. In other words, the apparent differences between pH of cancer tissues in comparison with healthy texture is potentially a suitable trigger for the fabrication of proprietary drug delivery systems.[59]

Cancer cells are reprogramming uncontrolled cells that use anaerobic metabolic pathway for the production of ATP molecules even in the presence of oxygen. This change in the energy production pathway is an intelligent tactic employed by cancer cells to convert the glycolytic intermediates through specific approaches into the various types of biological macromolecules like nucleosides and amino acids to facilitate the production of organelles and macromolecules needs for the new cells. The anaerobic metabolism often encountered in cancer cells is accompanied by an increase in the amounts of lactic acid

concentration in the cells, ultimately leading to extracellular tumor acidosis. It means that cancer cells maintain their normal intracellular pH (7.4) by excreting the excess protons to the extracellular matrix through the upregulation of several proton extrusion mechanisms and thus the extracellular microenvironment of the cancer cells is slightly acidic (6.5–7).[60,61]

Based on this difference in pH of cancer and healthy tissues, different types of pH-responsive nano-systems are introduced which can respond to the pH change by using cleavable linkers or through applying the charge conversion components.[62]

Based on this feature of the cancer tissues, in this research, a smart pH-responsive nano theranostic capsule with a mean size of about 43 nm was fabricated for delivering anti-cancer drugs. This nanocapsule is constructed based on the supramolecular structure of CD molecules that contains three polymeric layers which are located around the magnetic core of the nano-system. This magnetic core also donates a
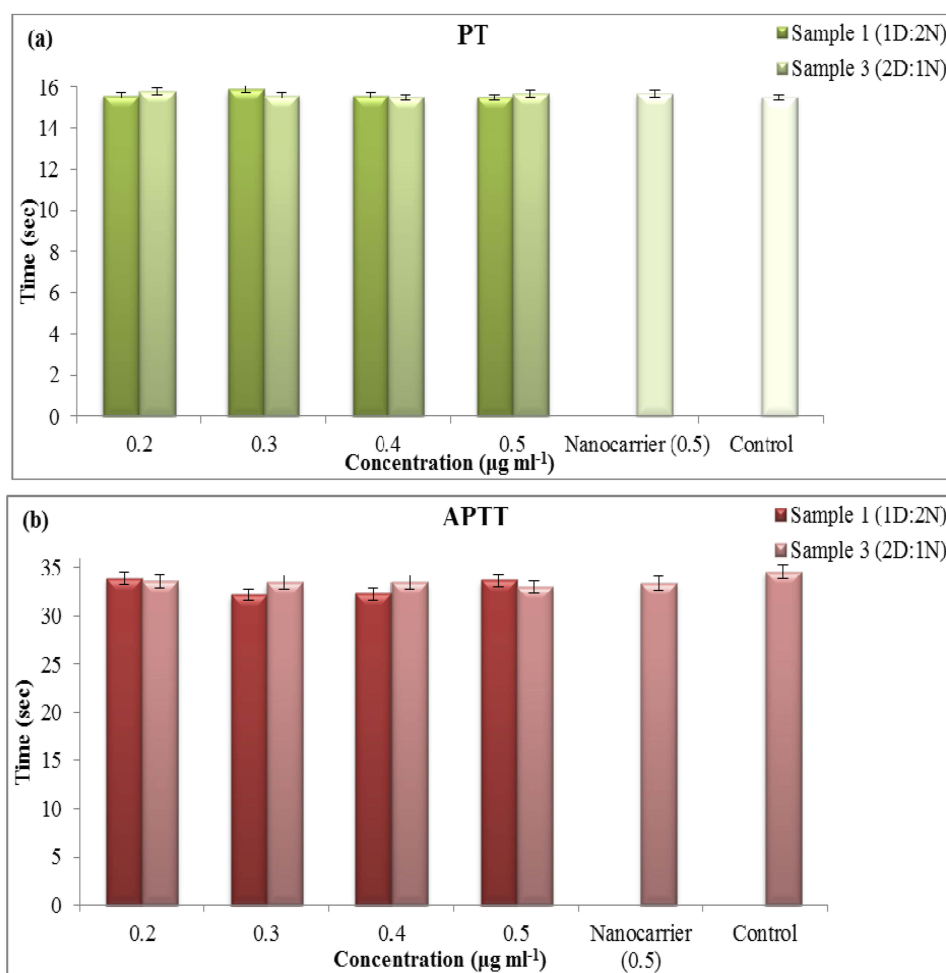
Figure 14 Effect of different concentrations of nanocapsules on (**A**) PT and (**B**) APTT.

diagnostic feature to this nano-system. This is a new type of supramolecular structure with a high capacity for drug loading and also shows on/off switching drug release behavior which is originated from the inclusion complex between cyclodextrin components and SDNs. This nano-system could show a hydrogel-like behavior, and release its cargos in a swelling like manner in acidic pH without losing its structural framework.

As it has been mentioned before, use of stimuli agents in the structure of nano-platforms, induces on/off switching behavior, which implies that these types of drug delivery systems could release their component just in the presence of a specific situation. The presence of the stimuli situations, turns to a change in the structure of the nano-system that leads to release the drugs entitled "switch on", while by removing that situation no release occurs from the nano-system, which is entitled "switch off". These nanocarriers are a class of smart nano-systems with the ability to maintain their structure after stimulation. According to this feature, several species of nano-systems had been introduced by researchers in which extrinsic (UV and magnetic) or intrinsic (pH, redox and temperature) stimuli agents were used.[39,63–65]

The other advantage of this nanocarrier is its high loading capacity which is near about 160% for doxorubicin and also its sustain release behavior during 14 days. So far, several types of nano-systems with different strategies have been chosen for delivering doxorubicin to its targeted site. For example in 2018, Li et al introduced a pH-responsive supramolecular nano theranostics based on pillararene that showed about 3.67% loading efficiency and pH-dependent release pattern with about 20% drug release in pH 6.5 and 70% in pH 4.[66] Wallat et al applied a fluorous polymeric micelle as a vehicle for DOX, in which drugs were covalently conjugated to the micelles via a pH-responsive hydrazone linkage and showed about

20% drug release during 50 h at pH 5.[67] By comparing the drug loading and releasing behavior of nanocapsule studied in this research with other similar studies,[68–70] it could be concluded that this nanocarrier has much higher loading efficiency and also could show better performance in response to the acidic environment of cancer tissue for releasing drugs.

As an intravenous injectable drug carrier, the effect of nanocapsules on RBC, and blood immune system were also evaluated using different tests that revealed the hemocompatibility of the nanocapsules even in the presence of drug molecules. The cytotoxicity of the nanocapsules (with/without drug components) was also assessed in normal and cancer cells. The results of cytotoxicity tests indicated that drug-loaded nanocapsules do not affect normal cells while they show distinctive cytotoxicity on MCF7 cancer cells after 48 h that can be considered as an evidence for confirming the pH-responsive behavior of the nanocapsules. Overall, according to these in vitro tests, this nanocapsule could be introduced as a smart pH-responsive drug nanocarrier with switchable controlled release property which can be used for cancer treatment.

Finally, the attendance of Fe_2O_3 nanoparticles in the core of nanocapsule turns to recommend it as a diagnostic agent for magnetic resonance imaging of the targeted region that can enhance the quality of the imaging by affecting the T_1 and T_2 relaxation times.[71]

Conclusion

Application of smart nano-systems in pharmacy with the aim of cancer treatment is the subject of many scientific studies in the last decade. In this research, a new type of pH-responsive nanocapsule was fabricated with the ability of on/off switching drug release to be used as a nano theranostic agent for cancer simultaneous diagnosis and therapy. The nanocapsule was consisted of three polymeric layers including polymeric beta-cyclodextrin, sulfadiazine functionalized polyacrylic acid and beta-cyclodextrin attached to the polyethylenimine, in which the inclusion complex formed between cyclodextrin components and sulfadiazine donate a pH-responsive property to the nano-system. The physicochemical and in vitro biological properties of the nanocapsule were confirmed by different tests. Results revealed that this is a biocompatible nanocapsule with about 43 nm size and −42 mV surface charge, which show 50–160% drug loading capacity and also a controllable sustained drug release behavior. Representing the cytotoxicity effect against cancer cells at very low concentrations along with the pH-responsive drug release pattern and also an improvement in the therapeutic efficiency of the drug, this nanocapsule is proposed as an possible therapeutic agent that can eliminate the side effects on normal cells, as well as, a significant reduction in the dose of drug usage leading to prevention of drug resistance behavior of cancer cells. Combination of the therapeutic features of the nanocapsule with the diagnostic property of the magnetic nanoparticles which are presented in the core of this nano-system, introduce this new type of nanocarrier as a theranostic candidate for simultaneous diagnosis and therapy of cancer.

Ethics approval

It is certified that the participant in this study (RBC aggregation) has provided the Ethics Committee with the written informed consent and the ethics committee has approved the consent process and the whole process of working with RBC. In addition, we confirm that the donors' data are anonymized and are maintained with confidentiality.

Disclosure

We confirm that there are no known conflicts of interest associated with this publication and there has been no significant financial support for this work that could have influenced its outcome.

References

1. Kumari P, Ghosh B, Biswas S. Nanocarriers for cancer-targeted drug delivery. *J Drug Target*. 2016;24(3):179–191. doi:10.3109/1061186X.2015.1051049
2. Estanqueiro M, Amaral MH, Conceicao J, Lobo JMS. Nanotechnological carriers for cancer chemotherapy: the state of the art. *Colloids Surf B*. 2015;126:631–648. doi:10.1016/j.colsurfb.2014.12.041
3. McQuade RM, Bornstein JC, Nurgali K. Anti-colorectal cancer chemotherapy-induced diarrhoea: current treatments and side-effects. *Int J Clin Exp Med*. 2014;5:393–406. doi:10.4236/ijcm.2014.57054
4. Chowdhury P, Nagesh PK, Hatami E, et al. Tannic acid-inspired paclitaxel nanoparticles for enhanced anticancer effects in breast cancer cells. *J Colloid Interface Sci*. 2019;535:133–148. doi:10.1016/j.jcis.2018.09.072

5. Zhu Y, Liao L. Applications of nanoparticles for anticancer drug delivery: a review. *J Nanosci Nanotechnol*. 2015;15:4753–4773. doi:10.1166/jnn.2015.10298

6. Qin SY, Zhang AQ, Cheng SX, Rong L, Zhang XZ. Drug self-delivery systems for cancer therapy. *Biomaterials*. 2017;112:234–247. doi:10.1016/j.biomaterials.2016.10.016

7. Moghanjoughi AA, Khoshnevis D, Zarrabi A. A concise review on smart polymers for controlled drug release. *Drug Deliv Transl Res*. 2016;6:333–340. doi:10.1007/s13346-015-0274-7

8. Karuppusamy C, Venkatesan P. Role of nanoparticles in drug delivery system: a comprehensive review. *Int J Pharm Sci Res*. 2017;9:318–325.

9. Koushik O, Rao Y, Kumar P, Karthikeyan R. Nano drug delivery systems to overcome cancer drug resistance—a review. *Nanomed Nanotechnol*. 2016;7(378):2–10.

10. Kalaydina RV, Bajwa K, Qorri B, Decarlo A, Szewczuk MR. Recent advances in "smart" delivery systems for extended drug release in cancer therapy. *Int J Nanomed*. 2018;13:4727–4745. doi:10.2147/IJN.S168053

11. Gu M, Wang X, Toh TB, Chow EKH. Applications of stimuli-responsive nanoscale drug delivery systems in translational research. *Drug Dscov Today*. 2018;23(5):1043–1052. doi:10.1016/j.drudis.2017.11.009

12. Ramasamy T, Ruttala HB, Gupta B, et al. Smart chemistry-based nanosized drug delivery systems for systemic applications: a comprehensive review. *J Control Release*. 2017;258:226–253. doi:10.1016/j.jconrel.2017.04.043

13. Goyal AK, Rath G, Faujdar C, Malik B. Application and perspective of pH-responsive nano drug delivery systems. In: *Applications of Targeted Nano Drugs and Delivery Systems*. Elsevier; 2019:15–33.

14. Jahandar M, Zarrabi A, Shokrgozar MA, Mousavi H. Synthesis, characterization and application of polyglycerol coated Fe₃O₄ nanoparticles as a nano-theranostics agent. *Mater Res Express*. 2015;2 (12):125002. doi:10.1088/2053-1591/2/12/125002

15. Li L, Chen C, Liu H, et al. Multifunctional carbon–silica nanocapsules with gold core for synergistic photothermal and chemo-cancer therapy under the guidance of bimodal imaging. *Adv Func Mater*. 2016;26(24):4252–4261. doi:10.1002/adfm.201600985

16. AbdElhamid AS, Zayed DG, Helmy MW, et al. Lactoferrin-tagged quantum dots-based theranostic nanocapsules for combined COX-2 inhibitor/herbal therapy of breast cancer. *Nanomedicine*. 2018;13 (20):2637–2656. doi:10.2217/nnm-2018-0196

17. Bobo D, Robinson KJ, Islam J, Thurecht KJ, Corrie SR. Nanoparticle-based medicines: a review of FDA-approved materials and clinical trials to date. *Pharm Res*. 2016;33(10):2373–2387. doi:10.1007/s11095-016-1958-5

18. Mora-Huertas CE, Fessi H, Elaissari A. Polymer-based nanocapsules for drug delivery. *Int J Pharm*. 2010;385(1–2):113–142. doi:10.1016/j.ijpharm.2009.10.018

19. Bentz KC, Savin DA. Hollow polymer nanocapsules: synthesis, properties, and applications. *Polym Chem*. 2018;9(16):2059–2081. doi:10.1039/C8PY00142A

20. Zhang M, Nowak M, de Molina M, et al. Synthesis of oil-laden poly (ethylene glycol) diacrylate hydrogel nanocapsules from double nanoemulsions. *Langmuir*. 2017;33(24):6116–6126. doi:10.1021/acs.langmuir.7b01162

21. Erdoğar N, Akkın S, Bilensoy E. Nanocapsules for drug delivery: an updated review of the last decade. *Recent Pat Drug Deliv Formul*. 2018;12(4):252–266. doi:10.2174/1872211313666190123153711

22. Shutava TG, Livanovich KS, Sharamet AA. Layer-by-layer films of polysaccharides modified with polyethylene glycol and dextran. *Colloids Surf B*. 2019;173:412–420. doi:10.1016/j.colsurfb.2018.10.009

23. Song XQ, Tao C, Li W, Wang JX, Le Y, Zhang JJ. Preparation of reduction-responsive camptothecin nanocapsules by combining nano-precipitation and in situ polymerization for anticancer therapy. *Pharmaceutics*. 2018;10(4):173. doi:10.3390/pharmaceutics10040173

24. Iyisan B, Landfester K. Modular approach for the design of smart polymeric nanocapsules. *Macromol Rapid Commun*. 2019;40 (1):1800577. doi:10.1002/marc.201800577

25. Vilela C, Figueiredo AR, Silvestre AJ, Freire CS. Multilayered materials based on biopolymers as drug delivery systems. *Expert Opin Drug Deliv*. 2017;14(2):189–200. doi:10.1080/17425247.2016.1214568

26. Gharibzahedi SM, Jafari SM. Nanocapsule formation by cyclodextrins. In: *Nanoencapsulation Technologies for the Food and Nutraceutical Industries*. Academic Press, Elsevier; 2017:187–261.

27. Jahed V, Zarrabi A, Bordbar AK, Hafezi MS. NMR (1H, ROESY) spectroscopic and molecular modelling investigations of supramolecular complex of β-cyclodextrin and curcumin. *Food Chem*. 2014;165:241–246. doi:10.1016/j.foodchem.2014.05.094

28. Swaminathan S, Trotta F. Cyclodextrin nanosponges1. *Nanosponges*. 2019;27–57.

29. Rajendiran N, Siva S. Inclusion complex of sulfadimethoxine with cyclodextrins: preparation and characterization. *Carbohydr Polym*. 2014;101:828–836. doi:10.1016/j.carbpol.2013.10.016

30. Delrivo A, Zoppi A, Granero G, Longhi M. Studies of ternary systems of sulfadiazine with β-cyclodextrin and aminoacids. *Ars Pharm*. 2016;57(4):167–176.

31. Delrivo A, Zoppi A, Longhi MR. Interaction of sulfadiazine with cyclodextrins in aqueous solution and solid state. *Carbohydr Polym*. 2012;87(3):1980–1988. doi:10.1016/j.carbpol.2011.10.025

32. Lyon JL, Fleming DA, Stone MB, Schiffer P, Williams ME. Synthesis of Fe oxide core/Au shell nanoparticles by iterative hydroxylamine seeding. *Nano Lett*. 2004;4:719–723. doi:10.1021/nl035253f

33. Mousavi H, Movahedi B, Zarrabi A, Jahandar M. A multifunctional hierarchically assembled magnetic nanostructure towards cancer nano-theranostics. *RSC Adv*. 2015;5(94):77255–77263. doi:10.1039/C5RA16776K

34. Bao F, Yao JL, Gu RA. Synthesis of magnetic Fe₂O₃/Au core/shell nanoparticles for bioseparation and immunoassay based on surface-enhanced Raman spectroscopy. *Langmuir*. 2009;25(18):10782–10787. doi:10.1021/la901337r

35. Tripodo G, Wischke C, Neffe AT, Lendlein A. Efficient synthesis of pure monotosylated beta-cyclodextrin and its dimers. *Carbohydr Res*. 2013;381:59–63. doi:10.1016/j.carres.2013.08.018

36. Fragoso A, Sanromà B, Ortiz M, O'Sullivan CK. Layer-by-layer self-assembly of peroxidase on gold electrodes based on complementary cyclodextrin–adamantane supramolecular interactions. *Soft Matter*. 2009;5(2):400–406. doi:10.1039/B813754D

37. Pun SH, Bellocq NC, Liu A, et al. Cyclodextrin-modified polyethylenimine polymers for gene delivery. *Bioconjug Chem*. 2004;15 (4):831–840. doi:10.1021/bc049891g

38. Raut SY, Manne AS, Kalthur G, Jain S, Mutalik S. Cyclodextrins as carriers in targeted delivery of therapeutic agents: focused review on traditional and inimitable applications. *Curr Pharm Des*. 2019;25 (4):444–454. doi:10.2174/1381612825666190306163602

39. Wajs E, Nielsen TT, Larsen KL, Fragoso A. Preparation of stimuli-responsive nano-sized capsules based on cyclodextrin polymers with redox or light switching properties. *Nano Res*. 2016;9(7):2070–2078. doi:10.1007/s12274-016-1097-7

40. Teranishi R, Matsuda T, Yuba E, Kono K, Harada A. Sonodynamic therapeutic effects of sonosensitizers with different intracellular distribution delivered by hollow nanocapsules exhibiting cytosol specific release. *Macromol Biosci*. 2019;1800365. doi:10.1002/mabi.201800365

41. Zhou J, Li T, Zhang C, Xiao J, Cui D, Cheng Y. Charge-switchable nanocapsules with multistage ph-responsive behaviours for enhanced tumour-targeted chemo/photodynamic therapy guided by nir/mr imaging. *Nanoscale*. 2018;10(20):9707–9719. doi:10.1039/c8nr00994e

42. Islami M, Zarrabi A, Tada S, Kawamoto M, Isoshima T, Ito Y. Controlled quercetin release from high-capacity-loading hyperbranched polyglycerol-functionalized graphene oxide. *Int J Nanomed*. 2018;2018(13):6059. doi:10.2147/IJN.S178374

43. Zhang C, Bu W, Ni D, et al. Synthesis of iron nanometallic glasses and their application in cancer therapy by a localized Fenton reaction. *Angew Chem Int Ed*. 2016;55:2101–2106. doi:10.1002/anie.201510031

44. Assadi Z, Emtiazi G, Zarrabi A. Novel synergistic activities of tetracycline copper oxide nanoparticles integrated into chitosan micro particles for delivery against multiple drug resistant strains: generation of reactive oxygen species (ROS) and cell death. *J Drug Deliv Sci Technol*. 2018;44:65–70. doi:10.1016/j.jddst.2017.11.017

45. Tan A, Hong L, Du JD, Boyd BJ. Self-assembled nanostructured lipid systems: is there a link between structure and cytotoxicity? *Adv Sci*. 2019;6(3):1801223. doi:10.1002/advs.v6.3

46. Zarrabi A, Shokrgozar MA, Vossoughi M, Farokhi M. In vitro bio-compatibility evaluations of hyperbranched polyglycerol hybrid nanos-tructure as a candidate for nanomedicine applications. *J Mater Sci Mater Med*. 2014;25(2):499–506. doi:10.1007/s10856-013-5094-z

47. Mostaghasi E, Zarepour A, Zarrabi A. Folic acid armed Fe₃O₄-HPG nanoparticles as a safe nano vehicle for biomedical theranostics. *J Taiwan Inst Chem Eng*. 2018;82:33–41. doi:10.1016/j.jtice.2017.11.004

48. Zhang S, Qi Y, Yang H, Gong M, Zhang D, Zou L. Optimization of the composition of bimetallic core/shell Fe₂O₃/Au nanoparticles for MRI/CT dual-mode imaging. *J Nanopart Res*. 2013;15:2023. doi:10.1007/s11051-013-2023-5

49. Li K, Lai Y, Zhang W, Jin L. Fe₂O₃@Au core/shell nanoparticle-based electrochemical DNA biosensor for Escherichia coli detection. *Talanta*. 2011;84(3):607–613. doi:10.1016/j.talanta.2010.12.042

50. Gidwani B, Vyas A. Synthesis, characterization and application of epichlorohydrin-β-cyclodextrin polymer. *Colloids Surf B*. 2014;114:130–137. doi:10.1016/j.colsurfb.2013.09.035

51. Li N, Wang N, Wu T, et al. Preparation of curcumin-hydroxypropyl-β-cyclodextrin inclusion complex by cosolvency-lyophilization procedure to enhance oral bioavailability of the drug. *Drug Dev Ind Pharm*. 2018;44 (12):1966–1974. doi:10.1080/03639045.2018.1505904

52. JIANG H, Zujin YANG, Xiantai ZHOU, Yanxiong FANG, Hongbing JI. Immobilization of β-cyclodextrin as insoluble β-cyclodextrin polymer and its catalytic performance. *Chin J Chem Eng*. 2012;20 (4):784–792. doi:10.1016/S1004-9541(11)60249-8

53. Todica M, Stefan T, Simon S, Balasz I, Daraban L. UV-vis and XRD investigation of graphite-doped poly (acrylic) acid membranes. *Turk J Phys*. 2014;38(2):261–267. doi:10.3906/fiz-1305-16

54. Liakos IL, Iordache F, Carzino R, et al. Cellulose acetate-essential oil nanocapsules with antimicrobial activity for biomedical applications. *Colloids Surf B*. 2018;172:471–479. doi:10.1016/j.colsurfb.2018.08.069

55. Gao C, Tang F, Gong G, et al. pH-responsive prodrug nanoparticles based on a sodium alginate derivative for selective co-release of doxorubicin and curcumin into tumor cells. *Nanoscale*. 2017;9 (34):12533–12542. doi:10.1039/c7nr03611f

56. Hajji S, Khedir SB, Hamza-Mnif I, et al. Biomedical potential of chitosan-silver nanoparticles with special reference to antioxidant, antibacterial, hemolytic and *in vivo* cutaneous wound healing effects. *Biochimica et Biophysica Acta (BBA)*. 2019;1863(1):241–254. doi:10.1016/j.bbagen.2018.10.010

57. Ray S, Sinha P, Laha B, Maiti S, Bhattacharyya UK, Nayak AK. Polysorbate 80 coated crosslinked chitosan nanoparticles of ropinir-ole hydrochloride for brain targeting. *J Drug Deliv Sci Tec*. 2018;48:21–29. doi:10.1016/j.jddst.2018.08.016

58. Cheng H-B, Zhang Y-M, Liu Y, Yoon J. Turn-on supramolecular host-guest nanosystems as theranostics for cancer. *Chem*. 2019;5 (3):553–574. doi:10.1016/j.chempr.2018.12.024

59. Webb BA, Chimenti M, Jacobson MP, Barber DL. Dysregulated pH: a perfect storm for cancer progression. *Nat Rev Cancer*. 2011;11 (9):671–677. doi:10.1038/nrc3110

60. Chen LQ, Pagel MD. Evaluating pH in the extracellular tumor microenvironment using CEST MRI and other imaging methods. *Adv Radiol*. 2015;2015:1–25. doi:10.1155/2015/206405

61. Kanamala M, Wilson WR, Yang M, Palmer BD, Wu Z. Mechanisms and biomaterials in pH-responsive tumour targeted drug delivery: a review. *Biomaterials*. 2016;85:152–167. doi:10.1016/j.biomaterials.2016.01.061

62. Thongchaivetcharat K, Jenjob R, Seidi F, Crespy D. Programming pH-responsive release of two payloads from dextran-based nano-capsules. *Carbohydr Polym*. 2019;217:217–223. doi:10.1016/j.carbpol.2019.04.023

63. Lv SN, Cheng CJ, Song YY, Zhao ZG. Temperature-switched con-trolled release nanosystems based on molecular recognition and poly-mer phase transition. *RSC Adv*. 2015;5(5):3248–3259. doi:10.1039/C4RA11075G

64. Liu F, Huang P, Huang D, et al. Smart "on-off" responsive drug delivery nanosystems for potential imaging diagnosis and targeted tumor therapy. *Chem Eng J*. 2019;365:358–368. doi:10.1016/j.cej.2019.02.037

65. Wajs E, Nielsen TT, Larsen KL, Fragoso A. Template-assisted pre-paration of permeable nanocapsules from complementary cyclodex-trin and adamantane–appended biocompatible dextran polymers. *Macromol Mater Eng*. 2015;300(9):878–884. doi:10.1002/mame.v300.9

66. Li H, Wei R, Yan GH, et al. Smart self-assembled nanosystem based on water-soluble pillararene and rare-earth-doped upconversion nano-particles for ph-responsive drug delivery. *ACS Appl Mater Interfaces*. 2018;10(5):4910–4920. doi:10.1021/acsami.7b14193

67. Wallat JD, Harrison JK, Pokorski JK. ph responsive doxorubicin delivery by fluorous polymers for cancer treatment. *Mol Pharm*. 2018;15(8):2954–2962. doi:10.1021/acs.molpharmaceut.7b01046

68. Teranishi R, Matsuki R, Yuba E, Harada A, Kono K. Doxorubicin delivery using ph and redox dual-responsive hollow nanocapsules with a cationic electrostatic barrier. *Pharmaceutics*. 2017;9(1):4. doi:10.3390/pharmaceutics9010004

69. Lu S, Xu L, Kang ET, Mahendran R, Chiong E, Neoh KG. Co-delivery of peptide-modified cisplatin and doxorubicin via mucoad-hesive nanocapsules for potential synergistic intravesical chemother-apy of non-muscle-invasive bladder cancer. *Eur J Pharm Sci*. 2016;84:103–115. doi:10.1016/j.ejps.2016.01.013

70. Zhao J, Yang H, Li J, Wang Y, Wang X. Fabrication of pH-responsive PLGA (UCNPs/DOX) nanocapsules with upconversion luminescence for drug delivery. *Sci Rep*. 2017;7(1):18014. doi:10.1038/s41598-017-16948-4

71. Zarepour A, Zarrabi A, Khosravi A. Spions as nano-theranostics agents. In: *SPIONs as Nano-Theranostics Agents*. Singapore: Springer; 2017:1–44.